Locoregional Confinement and Major Clinical Benefit of 188 Re-Loaded CXCR4-Targeted Nanocarriers in an Orthotopic Human to Mouse Model of Glioblastoma

Delphine Séhédic, Igor Chourpa, Clément Tétaud, Audrey Griveau, Claire Loussouarn, Sylvie Avril, Claire Legendre, Nicolas Lepareur, Didier Wion, François Hindré, et al.

IVYSPRING INTERNATIONAL PUBLISHER

Theranostics

2017; 7(18): 4517-4536. doi: 10.7150/thno.19403

Research Paper

Locoregional Confinement and Major Clinical Benefit of ^{188}Re-Loaded CXCR4-Targeted Nanocarriers in an Orthotopic Human to Mouse Model of Glioblastoma

Delphine Séhédic[1], Igor Chourpa[5], Clément Tétaud[1, 3], Audrey Griveau[1], Claire Loussouarn[1], Sylvie Avril[1], Claire Legendre[1], Nicolas Lepareur[6], Didier Wion[7], François Hindré[1, 3], François Davodeau[4], Emmanuel Garcion[1, 2, 3]✉

1. CRCINA, INSERM, Université de Nantes, Université d'Angers, 49933 Angers, France;
2. PACeM, "Plateforme d'Analyses Cellulaires et Moléculaires", Université d'Angers, 49933 Angers, France;
3. PRIMEX, "Plateforme de Radiobiologie et d'Imagerie EXperimentale", Université d'Angers, 49933 Angers, France;
4. CRCINA, INSERM, Université d'Angers, Université de Nantes, 44035 Nantes, France;
5. Université Tours, EA6295, "Nanomédicaments et Nanosondes", 37020 Tours, France;
6. Centre Regional de Lutte Contre le Cancer Eugène Marquis, Department of Nuclear Medicine, 35042 Rennes, France;
7. INSERM U1205, bâtiment modulaire 40-23, CEA 17 rue des Martyrs, 38054 Grenoble cedex, France.

✉ Corresponding author: Dr Emmanuel Garcion, emmanuel.garcion@univ-angers.fr CRCINA, INSERM U1232 Team 17, Design and Application of Innovative Local treatments in Glioblastoma (GLIAD), Université d'Angers, IBS - CHU, 4 Rue Larrey, F-49933 Angers, France +33 (0) 2 44 68 85 43

Received: 2017.01.30; Accepted: 2017.09.11; Published: 2017.10.12

Abstract

Purpose: Gold standard beam radiation for glioblastoma (GBM) treatment is challenged by resistance phenomena occurring in cellular populations well prepared to survive or to repair damage caused by radiation. Among signals that have been linked with radio-resistance, the SDF1/CXCR4 axis, associated with cancer stem-like cell, may be an opportune target. To avoid the problem of systemic toxicity and blood-brain barrier crossing, the relevance and efficacy of an original system of local brain internal radiation therapy combining a radiopharmaceutical with an immuno-nanoparticle was investigated.

Experiment design: The nanocarrier combined lipophilic thiobenzoate complexes of rhenium-188 loaded in the core of a lipid nanocapsule (LNC^{188}Re) with a function-blocking antibody, 12G5 directed at the CXCR4, on its surface. The efficiency of 12G5-LNC^{188}Re was investigated in an orthotopic and xenogenic GBM model of CXCR4-positive U87MG cells implanted in the striatum of Scid mice.

Results: We demonstrated that 12G5-LNC^{188}Re single infusion treatment by convection-enhanced delivery resulted in a major clinical improvement in median survival that was accompanied by locoregional effects on tumor development including hypovascularization and stimulation of the recruitment of bone marrow derived CD11b- or CD68-positive cells as confirmed by immunohistochemistry analysis. Interestingly, thorough analysis by spectral imaging in a chimeric U87MG GBM model containing CXCR4-positive/red fluorescent protein (RFP)-positive- and CXCR4-negative/RFP-negative-GBM cells revealed greater confinement of DiD-labeled 12G5-LNCs than control IgG2a-LNCs in RFP compartments.

Main conclusion: These findings on locoregional impact and targeting of disseminated cancer cells in tumor margins suggest that intracerebral active targeting of nanocarriers loaded with radiopharmaceuticals may have considerable benefits in clinical applications.

Key words: CXCR4, glioblastoma, radiation therapy, immuno-targeting, spectral imaging, macrophage; nanoparticle.

Introduction

Glioblastoma (GBM) is the most common and deadly primary brain tumor in adults (1). Conventional therapy consists of surgical resection followed by radiotherapy and chemotherapy, which improves patient survival but is rarely curative (2). The effectiveness of these treatments is limited by the blood-brain barrier (BBB) and the high sensitivity of brain tissue that limits high dose administration (3).

Ionizing radiation is the gold-standard adjuvant treatment for malignant gliomas. In order to limit toxicity to surrounding healthy tissue and enhance radiation damage to the tumor, different modes of locoregional drug delivery, such as stereotactic radiosurgery, are being developed. Locoregional delivery makes it possible to bypass BBB and to reduce the systemic toxicity of the treatment. Many clinical trials on GBM have demonstrated the interest of internal radioimmunotherapy using alpha radio-emitter (^{211}At-tenascin (4)) or beta-emitter (^{131}I-tenascin (5, 6), ^{90}Y-Abegrin (7), ^{188}Re-nimotuzumab (8)). Other studies have developed nanotechnologies to vectorize radioemitters in locoregional strategies (^{225}Ac-liposome (9), ^{186}Re-liposome (10), ^{188}Re-nanoliposome (11)). Our group developed lipid nanocapsules (LNCs) designed to incorporate radionuclides. LNCs are synthesized through a phase inversion process without any organic solvent and consist of a lipid core surrounded by a tensioactive shell (12). LNCs have been implanted in brain tumors using stereotactic injections for locoregional therapy: 50 nm LNCs were able to load a lipophilic complex of rhenium-188 (LNC^{188}Re; half-life: 16.9 h; β^- emitter: 2.12 MeV; γ emitter: 155 keV) for internal radiation therapy in malignant glioma, resulting in a median survival of up to 45 days after a single injection of LNC^{188}Re in an orthotopic 9L-glioma model (13). More recently, Vanpouille-Box *et al.* demonstrated the interest of fractionated radiotherapy and the importance of the mode of injection of LNC^{188}Re. These authors notably showed that a single injection followed by convection-enhanced delivery (CED) is the most effective protocol, with 80% longer survival of the animals (14).

The efficiency of radiotherapy depends on efficient targeting of tumor cells and causing minimum damage to healthy tissue, but also on the ability to bypass the intrinsic radioresistant proprieties of GBM. Indeed, in the last decade, a specific cell contingent, called glioma stem-like cells (GSCs) has been identified (15–19). These cells express neural stem cell markers (17, 20, 21), have the capacity for self-renewal and long term proliferation, and for the formation of neurospheres, like normal neural progenitors, but resist radiation through activation of the DNA damage checkpoint (22, 23). Recently, another receptor was identified as an interesting target for the development of GSC targeting therapy: the chemokine receptor CXCR4. It is the receptor of the chemokine CXCL12 (SDF-1α), and SDF-1/CXCR4 binding activates different signaling pathways including phosphatidylinositol-3 kinase (PI3K)/Akt and MAP-kinases signaling pathways. In adults, the SDF-1/CXCR4 axis plays a role in GBM development, tumor cell proliferation (24) and invasiveness via activation of matrix metalloproteinases (MMPs) (25). SDF-1 is secreted by the GSCs themselves but also by endothelial cells that have an autocrine and paracrine effect in the perivascular niche. The SDF-1/CXCR4 axis has been reported as a major regulator of the biological features of GSCs: self-renewal, proliferation, migration, angiogenesis and chemo- and radio-resistance. Overexpression of CXCR4 has been observed in GSCs that increase proliferation in response to exogenous SDF-1 (26). Furthermore, the SDF-1/CXCR4 axis plays a crucial role in vasculogenesis (27, 28). SDF-1/CXCR4 axis induced migration of CD11b+ myeloid cells, the precursors of tumor-associated macrophages (TAMs), to the tumor site. These cells expressed MMP and recruited endothelial cells to form new vessels (29). These monocytes also expressed CXCR4 on their surface. Thus, SDF-1/CXCR4 axis inhibition could have an impact on the development of tumor cells either by inhibition of the cell signaling involved in survival and proliferation or by acting on the micro environment (30).

In this study, the impact of the mutual action of intracerebral internal vectorized radiotherapy and active CXCR4-immunotargeting was investigated using 12G5-conjugated LNC^{188}Re in a xenogeneic and orthotopic glioma model of human U87MG cells expressing the CXCR4 receptor implanted in Scid mice. 12G5 is indeed a function-blocking antibody of the CXCR4 notably reported to inhibit SDF-1-induced glioblastoma cell proliferation (31). Special attention was paid to the therapeutic efficiency of the strategy and to the detailed behavior of locoregional nanocarriers.

Materials and Methods

Study design

This study was designed to investigate the interest of *in vivo* cellular targeting of rhenium-loaded lipid nanocapsules in a locoregional strategy. Anti-tumor efficacy and nanocarrier diffusion were investigated *in situ*. Nanocarrier synthesis required immunoglobulin production (Control IgG and Ig

directed to CXCR4) and coupling chemistry. The U87MG cell line was chosen as a model of tumor expansion *in vivo*. In order to overcome variations in CXCR4 expression in these cells, U87MG were transfected by a lentivirus coding for this receptor that results in the stable expression of the target CXCR4 in U87MG. Swiss Scid female mice were used for intra-cerebral implantation of GBM tumor cells. To demonstrate the efficiency of the anti-tumor strategy, treatments were administered through CED in one injection to obtain the largest possible distribution of the radiotherapeutic nanocarriers. MRI imagery enabled the characterization of the brain tumor tissue response to therapy. To understand the locoregional influence of target expression on the distribution of functionalized nanocarriers in the tumor parenchyma, a chimerical tumor model was developed from U87MG cells, one expressing CXCR4 and RFP (CXCR4+/RFP+) and the other not (CXCR4-/RFP-). Nanocarrier distribution was monitored by another fluorophore, different from the one used for the cells, and RFP/LNC colocalization in brain tumors was studied using fluorescence spectral imaging. Analyses were performed with dedicated software. Animals were then randomly assigned to different treatment groups within each cage and all the experiments were conducted under an approved protocol of the French Minister of Agriculture and the European Communities Council Directive of 24 November 1986 (86/609/EEC). The Ethics Committee for Animal Experimentation of the Region "Pays-de-la-Loire" approved the protocol used (permit number: CEEA.2012.60). All surgery was performed under ketamine/xylazine anesthesia, and all efforts were made to avoid suffering.

Tumor cell line culture and transfection

Human malignant glioma cell lines U87MG were purchased from the American Tissue Culture Collection (ATCC, Rockville, MD). Tumor cells were cultured in Dulbecco's Modified Eagle's medium 4.5 g/L glucose and L-glutamine (DMEM, Lonza, Verviers, Belgium) supplemented with 10% heat-inactivated fetal bovine serum (FBS, Lonza) and 1% antibiotic suspension (10 units/mL of penicillin, 10 mg/mL streptomycin and 25 µg/mL amphotericin B, Sigma-Aldrich, Saint-Louis, MO, USA). Tumor cells were incubated at 37°C with 5% CO_2 and 21% oxygenation.

In order to overcome variations in CXCR4 expression, the U87MG, known in our laboratory to not express this receptor, was transfected with two lentiviruses, one encoding CXCR4 (# LVP103, GenTarget Inc, San Diego, Ca) or the control lentivirus instead (CMV-Null-RB, GenTarget). The U87MG cells (10^4 cells/mL) harvested in the exponential growth phase were seeded on a 6-well plate in Eagle's minimal essential medium (EMEM, Lonza) with 10% FBS at 37°C in a humidified atmosphere with 5% CO_2. Lentiviral particles were harvested 24 h after seeding. The medium and the lentivirus were removed 24 h after infection. The infected tumor cells were kept in culture and selected 72 h after infection by adding Blasticidin (10 µg/mL) (Fisher Scientific, Illkirch, France).

Flow cytometry

U87MG were collected and dissociated using trypsin (Sigma-Aldrich). They were incubated with 5 µg/mL 12G5 (CD184, #555971, BD Pharmingen) or IgG2a (BD Biosciences, Le Pont-de-Claix, France) or immuno-LNCs (1/200) for 1 h at 4°C in PBS containing 5% FBS and 0.02% sodium azide. After three washes in PBS/FCS/azide, cells were incubated for 30 min at 4°C with 20 µg/mL FITC-conjugated goat anti-mouse IgG F(ab')2 fragment (Dako, Trappes, France) in PBS/FCS/azide. Following three more washes, cells were re-suspended in PBS with added 2% formaldehyde and 0.02% sodium azide before flow cytometry.

A BD FACSCalibur™ fluorescent-activated flow cytometer and BD CellQuest™ software (BD-Biosciences) were used for flow cytometry acquisition. Analysis was carried out using WinMDI 2.9 software (Scripps Institute, La Jolla, CA, USA).

Preparation of the ^{188}Re-SSS complex

^{188}Re as carrier-free Na [$^{188}ReO_4^-$] in physiological solution was obtained by saline elution and concentration of ^{188}W/^{188}Re generator (*Institut des Radioéléments*, Fleurus, Belgium). The ^{188}Re-SSS complex was prepared using the method of Lepareur *et al*. (32). Briefly, the ^{188}Re-SSS was obtained by the reaction of the ligand sodium dithiobenzoate (Organic synthesis platform, Rennes, France) with a freeze-dried formulation containing 30 mg sodium gluconate, 30 mg ascorbic acid, 40 mg potassium oxalate, and 4 mg $SnCl_2.2H_2O$ reconstituted in 0.5 mL of physiological serum. ~2 GBq of ^{188}Re-perrhenate ($^{188}ReO_4^-$; in 0.5 mL) was added, and the solution was mixed for 15 min at room temperature (RT). Next, 20 mg of sodium dithiobenzoate (in 0.5 mL; pH = 7) was added before the solution was heated at 100°C for 30 min, which enabled the formation of the ^{188}Re-SSS complex. Due to its preparation in aqueous media, the ^{188}Re-SSS complex was extracted with dichloromethane (1 mL) and washed three times with 1 mL of deionized water.

Nanocapsule formulation and characterization

Lipoïd® S75-3 (soybean lecithin at 69% of

phosphatidylcholine) and Solutol® HS15 (a mixture of polyethylene glycol 660 and polyethylene glycol 660 hydroxystearate) were supplied by Lipoïd Gmbh (Ludwigshafen, Germany) and BASH (Ludwigshafen, Germany), respectively. NaCl was supplied by Sigma (St-Quentin, Fallavier, France). Deionized water was obtained from a Milli-Q plus system (Millipore, Paris, France). Lipophilic Labrafac® CC (caprylic-capric acid triglycerides) was supplied by Gattefosse S.A. (Saint-Priest, France).

Studies were performed on 50 nm diameter LNCs. The LNCs were prepared according to the phase-inversion process described by Heurtault *et al.* (12) that follows the formation of an oil/water microemulsion containing an oily/fatty phase (triglycerides: Labrafac® WL 1349), a non-ionic hydrophilic surfactant (polyethylene glycol hydroxystearate: Solutol®HS15), and a lipophilic surfactant (lecithins: Lipoïd® S75-3). Briefly, 18.75 mg Lipoïd® S75-3, 211.5 mg Solutol® HS15, 257 mg Labrafac®, 22.25 mg NaCl and 740.5 mg deionized water were mixed by magnetic stirring. The ^{188}Re-SSS complex extracted with dichloromethane (1 mL) was then added to the other components of the emulsion. The organic solvent was removed by being heated at 60°C for 15 min. Three cycles of progressive heating and cooling between 60°C and 90°C were then carried out, followed by an irreversible shock caused by adding 3.125 mL of deionized water at 0°C. The suspension was then subjected to low magnetic stirring for 5 min. LNC^{188}Re were filtered using a 0.22 µm filter. The mean diameter, polydispersity index and zeta-potential were then determined using Malvern Zetasizer® Nano Series DTS 1060 (Malvern Instruments S.A., Worcestershire, UK).

Immunoglobulin purification and coupling of monoclonal antibodies to LNC^{188}Re

C1.18.4 (IgG2a producing cells) (TIB-11™) was obtained from ATCC and was cultivated in DMEM (Lonza) with 1% antibiotics and 10% horse serum. 12G5 was a kind gift from Dr. James Hoxie (University of Pennsylvania) and was cultivated in DMEM (Lonza) supplemented with 1% antibiotics, 8% NCTC (Lonza) and 20% FBS. Cells were plated in uncoated flasks at $2x10^4$ cell/mL and maintained at 37°C and 5% CO_2 until they reached 10^6 cell/mL, before being replated and immunoglobulins were removed from the supernatants.

The supernatant harvested from cultures of the 12G5 and TIB-11 hybridoma cell lines containing 12G5 and IgG2a isotype control monoclonal antibodies (mAbs), respectively, was concentrated using Amicon®Ultra (100 000 MWCO) according to the manufacturer's instructions (Millipore, Billerica, USA). Immunoglobulins were then purified by passage over a high performance HiTrap Protein G HP column (GE Healthcare, Orsay, France) followed by elution in acid conditions and immediate neutralization according to the manufacturer's instructions. MAbs buffer was changed by dialysis into PBS using overnight membrane dialysis (15 000 MWCO, SpectrumLabs, Rancho Domingez, CA, USA) and then concentrated with Amicon®Ultra centrifugal filter units (30 000 MWCO, Millipore). The concentration of antibodies was determined with a NanoDrop 2000 spectrophotometer (Thermo Scientific). For thiolation, mAbs was incubated in PBS with 2-iminothiolane (Traut's reagent, Fisher, Illkirch, France) at a mole/mole ratio of 1/40 (6.2 mg mAbs for 0.224 mg 2-iminothiolane in 1 mL PBS) under agitation for 1 h in the dark. Traut's reagent was eliminated by purification of relational medium on PD10 column (Sephadex™ G-25M, GE Healthcare, Buckinghamshire, UK).

MAbs were coupled to LNC^{188}Re according to method 2 described by Bourseau-Guilmain *et al*. (33). Briefly, DSPE-PEG_{2000}-maleimide (Avanti Polar Lipids, Alabaster, USA) solubilized in DPBS, was added to a solution of DPBS containing 8 mg of thiolated mAbs (12G5 and IgG2a) to obtain an equimolar concentration of 0.05 mM for the two reactive species (DSPE-PEG_{2000}-maleimide and thiolated mAbs) in a final volume of 2 mL. The solution was incubated overnight at RT under low agitation. A total of 170 mg of LNCs corresponding to 1.3 mL of LNC^{188}Re were added to the formed "lipo-immunoglobulins" for 1 h of incubation at 45°C. A 1.5 cm x 40 cm sepharose CL4-B column (Sigma-Aldrich) equilibrated with sterile water was used to separate the functionalized LNC^{188}Re-SSS from free micelles composed of free lipo-immunoglobulins. Fractions containing immnuno-LNC^{188}Re were pooled and concentrated on Amicon®Ultra (100 000 MWCO, Millipore, Billerica, USA) by centrifugation at 4000 rpm for 30 min. After concentration, immuno-LNC^{188}Re were diluted to a final concentration of 2.7 MBq in 10L. The mean diameter, polydispersity index and zeta potential were then determined using Malvern Zetasizer® Nano Series DTS 1060.

Turbidimetric measurements were performed to evaluate the concentrations of LNCs in the collected fractions. Micro-BCA protein assay (Pierce) was used according to the manufacturer's instructions with DO analysis at 580 nm to determine the corresponding concentrations of mAbs. The number of mAbs per LNC is the ratio of the total number of mAbs on the total number of LNCs. The total number of mAbs was estimated by mAb concentration (measured by

microBCA assay) multiplied by the fraction volume multiplied by Avogadro number. The total LNCs was estimated by LNC concentration (measured by turbidimetry) multiplied by the fraction volume divided by Labrafac® density and then, divided by 50nm LNC volume.

The radioactivity of each fraction was determined using a gamma counter (Packard Auto-Gamma 5000 series).

Western blot analysis

Total proteins were isolated from GBM cells by sonication in a lysis buffer composed of 50 mM HEPES, pH 7.5, 150 mM NaCl, 1 mM EDTA, pH 8, 2.5 mM EGTA, pH 7.4, 0.1% Tween 20, 10% glycerol, 0.1 mM sodium orthovanadate, 1 mM sodium fluoride, 10 mM glycerophosphate and 0.1 mM phenylmethylsulfonyl fluoride (PMSF). Proteins (20 µg) were resolved on 4–20% Mini-PROTEAN® TGX™ precast polyacrylamide gels (Bio-Rad, Marnes-la-Coquette, France) and transferred to an Amersham GE Healthcare PVDF membrane (0.45 µm pore size) (Fisher Scientific, Illkirch, France). The following antibodies were used: a rabbit anti-human Phospho-Akt (Ser473) (#4058, clone 193H12, Ozyme, St Quentin en Yvelines, France), rabbit anti-human Akt (#9272, Ozyme). They were diluted at a ratio of 1:1000 according to the manufacturer's instructions. Goat anti-Rabbit and anti-Mouse IgG Secondary Antibody, HRP conjugate (Fisher Scientific, Illkirch, France) was used at a dilution of 1:2000. Detection was performed on SuperSignal™ West Femto Maximum Sensitivity Substrate (Fisher Scientific, Illkirch, France) with a ChemiCapt 3000 imaging system (Vilber Lourmat, Marne-la-Vallée France).

Mouse models

All mouse experiments were approved by the Ethics of Animal Experiments of the Pays de la Loire committee (Permit No. CEEA. 2012.60; Authorization n°A 49-2012-04). Female CB17-SCID immune-deprived (CB-17/lcr-*Prkdc*^{scid}/Rj) mice aged 6-7 weeks were obtained from Janvier Labs (Le Genest Saint Isle, France). The animals were kept in polycarbonate cages in a room with controlled temperature (20-22°C), humidity (50-70%), and light (12 h light/dark cycles). Room air was renewed at the rate of 10 room air changes/h. Tap water and food were provided *ad libitum*.

Tumor cells for intracerebral implantation were trypsinized, counted, and checked for viability by trypan blue exclusion. The cells were washed twice with phosphate-buffered saline (PBS, Lonza) and suspended in EMEM (Lonza) with no FBS or antibiotics at a final concentration of $1x10^7$ cells/mL. The mice were anesthetized with an intraperitoneal injection of a solution containing 100mg/kg body weight of ketamine (Clorkétam 1000, Vétoquinol, Lure, France), and 13mg/kg body weight of xylazine (Rompun 2%, Bayer, Puteaux, France) in sterile water. Using a stereotactic head frame (Stoelting, Wood Dale, IL, USA) and a 10 µL Hamilton syringe (Hamilton® glass syringe 700 series RN) with a 32-G needle (Hamilton®), 5 µL of $5x10^4$ U87MG CXCR4 positive cells were injected into the mouse's right striatum. The coordinates used for the intracerebral injection were 0.5 mm anterior to the bregma, 2 mm lateral to the sagittal suture (right hemisphere), and 3 mm below the dura.

For the spectral imaging experiment, a cell suspension containing 7/10 of U87MG and 3/10 of U87MG CXCR4 positive cells at a concentration of $5x10^4$ in 5 µL was injected in the same way.

Tumors were implanted in 8-week-old female SCID mice. The efficacy of 12G5-LNC^{188}Re was assessed at a late stage of tumor progression, and to this end, the animals received internal radiotherapy on D12. The type of administration of treatments was CED at a final volume of 10 µL and a flow rate of 0.5 µL/min. The experiment comprised seven groups: a 12G5-LNC^{188}Re group (n = 6), IgG2a-LNC^{188}Re group (n = 7), LNC^{188}Re group (n = 7), 12G5-LNC group (n = 6), IgG2a-LNC group (n = 6), LNC group (n = 9), and a saline solution group (n = 6). We chose to set the injected activity at 2.7 MBq of LNC^{188}Re because it had been shown to be effective after a single injection in a previous animal model (13).

Animals were anesthetized as previously described. A volume of 10 µL was injected into the mouse striatum at a flow rate of 0.5 µL/min using a 10 µL syringe (Hamilton® glass syringe 700 series RN) with a 32-G needle (Hamilton®) connected to a pump (Harvard apparatus Pump II Elite, Les Ulis, France). For this purpose, the mice were immobilized in a stereotactic head frame. The coordinates used for CED were the same as previously described. Following the injection, the needle was left in place for an additional 5 min to avoid expulsion of the suspension from the brain during the removal of the syringe.

MRI of mice

Mice under isoflurane anesthesia (1.5-0.5%, O_2 0.5 L/min) were scanned using a Burker Biospec 70/20 device, operating at a magnetic field of 7T (Bruker, Wissembourg, France), equipped with a 1 H cryoprobe to assess tumor development. Mouse body temperature was maintained at 36.5-37.5°C by a feedback-regulated heating pad throughout the imaging protocol. Rapid anatomical proton images were obtained using a rapid acquisition with

relaxation enhancement (RARE) sequence [TR = 3200 ms; mean echo time (TE) = 21.3 ms; RARE factor = 4; FOV = 2 cm x 2 cm; matrix 256 x 256; 11 contiguous slices of 0.5 mm, Nex = 1].

Immunohistochemitry

Animals were sacrificed at three different points in the protocol: at day 12, corresponding to the characteristics of the tumor before treatment, at day 19, and at the end point. The brains of tumor-bearing animals were frozen at -30°C in isopentane cooled with liquid nitrogen and stored at -80°C. 14 µm cryosections were made using a cryostat Leica CM3050S and stored at -20°C. They were then fixed with methanol for 10 min at -20°C. For CD68 and inducible type-2 nitric oxide synthase (NOSII) immunostaining, sections were rehydrated with 1× PBS for 15 min and fixed with paraformaldehyde 4% (PFA) for 10 min at 4°C. For arginase-1 (Arg1), sections were fixed with 95% ethanol / 5% acetic acid for 20 min at -20°C. In order to block nonspecific sites, the sections were incubated for 45 min at RT in PBS containing 4% bovine serum albumin (BSA) or PBS / 4% BSA / 0.25% Triton for intracellular labeling and 10% normal goat serum, and washed three times with PBS. Sections were then incubated overnight at 4°C with primary antibodies diluted in 4% PBS/BSA: CD31 (1/200, #550274, BD Pharmingen), CD11b (1/200, #MCA74G, AbD Serotec), CXCR4 (1/200, #PA3-305, Thermo Scientific), MMP9 (1/1000, #ab38898, Abcam), Ki67 (1/1000, #ab16667, Abcam), IgG2a (1/320, #559073, BD Pharmingen), IgG2b (1/100, #559478, BD Pharmingen). In the same way, CD68 (1/200, #ab125212, Abcam), NOSII (1/200, #ABN26, Merck Millipore) and Arg1 (1/200, #ABC897, Merck Millipore) were diluted in PBS / 4% BSA / 0.25% Triton and sections were incubated as previously described. After three washes with PBS, primary antibodies were detected using a biotinylated anti-Rat, anti-Rabbit or anti-Mouse IgG secondary antibody (1/100, Vector Laboratories). After 1 h RT, the sections were washed three times with PBS. Sections were developed with FITC-conjugated secondary antibody (1/500, Streptavidine-FITC conjugate, Dako) after 45 min incubation at RT and mounted using Dako Fluorescent Mounting Medium (Dako). Labeled cryosections were analyzed under a fluorescent microscope (Axioscope® 2 optical). Quantifications were made using the MetaMorph®/MetaView™ computer image-analysis system.

Fluorescence spectral imaging

The distribution of the nanoparticles in the brain tumors was monitored using a fluorescence spectral imaging technique. This technique, which consists of recording full spectra from different points of scanned sample regions, makes it possible to distinguish the fluorescence signal of numerous co-localized fluorophores and/or their different molecular states (34,35). In the present work, we used spectral imaging to simultaneously monitor the autofluorescence of tissues, the fluorescence of RFP-labeled cells and that of LNCs fluorescently labeled with DiD dye.

To this end, 50 nm LNCs loaded with DiD were prepared using the inversion phase process described by Hirsjärvi *et al.* (36). Briefly, Solutol®, Lipoïd®, Labrafac®, NaCl® and water were mixed and DiD in acetone (Invitrogen, Cergy Pontoise, France) was added to this mixture. The concentration of DiD was 3 mg/g (weight ratio dye/Labrafac®). Acetone was evaporated by heating for 15 min at 60°C under stirring. As described above, a micro-emulsion o/w was performed after three cycles of heating/cooling between 60°C and 90°C and fixed by adding water at 0°C.

DiD-LNCs were coupled with 12G5 and IgG2a mAbs in a similar way to LNC^{188}Re and were injected by CED into the right striatum of the chimeric tumor (U87MG/U87MG CXCR4+, (70:30)) of cancer-carrying mice. Four groups of four animals received the following treatment: DiD-LNCs, 12G5-DiD-LNCs, IgG2a-DiD-LNCs, saline solution. 24 h after injection, the animals were sacrificed and the brains of tumor bearing mice were removed. Brain cryosections 14 µm thick were made and placed on glass slides, with no additional treatment.

The fluorescence spectral maps were recorded by scanning selected regions of the cryosections under a ×10 objective of a confocal microspectrometer (Labram, Horiba SA, France) equipped with a 300 line/mm diffraction grating and an air-cooled CCD detector. The fluorescence spectra were excited using the 488 nm line of an Ar^+ laser (Melles Griot, France). The laser power on the sample was reduced to ~30 µW. Spectra were acquired with a 3 µm step size at 0.02 s intervals per spectrum.

The maps were recorded and treated using LabSpec software (Horiba SA, France). Briefly, each experimental spectrum was fitted with a proportional sum of model spectra characteristic of the molecular composition of the samples, described below. The fitting coefficients were used to generate parametric maps describing the distribution of the corresponding fluorophores.

Statistical analysis

GraphPad Prism 5 Version 5.03 was used for data analysis. Statistical analyses were performed using one- or two-way analysis of variance (ANOVA)

while statistical significance for survival experiments was determined using the log rank test. The tests were considered as significant when *p*-values were less than 0.05 and highly significant when *p*-values were less than 0.001.

Results

CXCR4-recognizing immuno-nanoparticle synthesis and characterization

To obtain nanoparticles that matched our requirements and the prerogatives of intracerebral internal vectorized radiotherapy and active CXCR4-immunotargeting, lipid immunonanocapsules were formulated and characterized.

The physical-chemical proprieties of LNCs are presented in Table 1. Blank LNCs were obtained with a mean size of 55.41±3.6 nm while displaying a very narrow distribution (PDI < 0.1). LNC^{188}Re were measured at 58.12±2.5 nm, and were also highly monodisperse. Post-insertion, immunoglobulin enhanced LNC size by about 5 to 8 nm for blank LNCs (12G5-LNC = 60.44±2.8 nm and IgG2a-LNCs = 63.48±3.8 nm) and by about 17 to 19 nm for LNC^{188}Re (12G5-LNC^{188}Re = 77.25±6.8 nm and IgG2a-LNC^{188}Re = 74.81±6.5 nm). The polydispersity index exceeded that of non-functionalized LNC (PDI < 0.1), thus presenting a slightly higher degree of heterogeneity but still around a 0.2 threshold for reliability in terms of uniform LNC primary size (of about 50-100 nm) with no aggregation and no agglomeration (37). Zeta-potentials were negative for all nanocarriers but were reduced by immunoglobulin post-insertion and to a greater extent for immuno-LNC^{188}Re. The greater increase in the size of LNC when lipophilic complexes of rhenium are encapsulated could be explained by the steric hindrance of the heart of the nanoparticles in which the fatty acid chains of the immunoglobulin-conjugated DSPE-PEG monomers are anchored, but also by the surfactant properties of the monomers effectively post-inserted depending on the conditions (Table 1). The reduction in zeta potential, which is greater in the presence of ^{188}Re-SSS complex, combined with the increase in size strongly supports surface functionalization of the newly formulated nanocarriers by the added immunoglobulins (Table 1).

The immuno-LNC^{188}Re manufacturing process was divided in two phases: on the one hand, formation of the ^{188}Re-SSS complex, and on the other hand, the formation of LNCs accompanied by a post-insertion/purification/concentration procedure. The formation of the ^{188}Re-SSS complex follows the reaction described by Lepareur *et al*. (32). Perrhenate ($^{188}ReO_4$) was reduced to form an intermediate compound that reacts with the sodium salt of a diothiobenzoate ligand to give the neutral complex [$^{188}Re(PhCS_3)_2(PhCS_2)$]. This ^{188}Re-SSS was added to other LNC excipients to form LNC^{188}Re. After formation, thiolated antibodies (12G5 or IgG2a) were incubated with blank LNCs or LNC^{188}Re for 1 h at 45°C. Post-insertion time was reduced compared to the process described by Bourseau *et al*. (33) because of ^{188}Re half-life. Antibody stability was evaluated to check if heating at 45°C destroyed the antibody and its recognition of its receptor CXCR4. Flow cytometry analysis showed that heating did not affect 12G5 recognition capacity (Figure 1A). After incubation, immuno-LNC^{188}Re were purified on a sepharose column. Fractions (1 mL) were harvested and antibody and LNC concentrations and activity were measured for each fraction (Figure 1B). There were ~10 antibodies on each LNC, thus representing a w/w ratio of ~4% (Table 1). Maximum measured activity correlated with fractions containing immuno-LNC. Next, the positive fractions were concentrated to obtain a final concentration of 2.7 MBq in 10 µL.

Table 1. Physical-chemical properties (size, polydispersity index (PDI), zeta-potential) of the different LNC. Differences between classical LNCs and immuno-LNCs: **p*-values < 0.05 Differences between LNC^{188}Re and rhenium-free LNC: $^{\#}p$-value < 0.05.

	Size (nm)	PdI	Zeta-potential (mV)	Antibodies per LNC
LNC	55.41±3.6	0.03±0.01	-4.51±0.75	
12G5-LNC	60.44±2.8	0.24±0.15	-13.87±2.0	35±20
IgG2a-LNC	63.48±3.8	0.26±0.01	-14.95±2.2	15±2
LNC-^{188}Re	58.12±2.5	0.05±0.03	-8.37±3.5	
12G5-LNC^{188}Re	77.25±6.8	0.21±0.04	-24.77±4.9	13±3
IgG2a-LNC^{188}Re	74.81±6.5	0.21±0.03	-26.23±8.3	10±5

Immunospecificity was checked for 12G5-LNC to determine the ability of the post-inserted antibody to effectively recognize its receptor. The flow cytometry analysis in Figure 1C shows that 12G5-LNCs efficiently recognized CXCR4 but with lower signal intensity than free 12G5 through the technology we used (amplification with a secondary antibody as for classical immunostaining). This difference is likely due to a distinct mode of presentation of the antibody at the surface of the LNCs and steric hindrance around the LNCs, which partly affected not only recognition of CXCR4 positive cells but also of the technical parameters needed to reveal this recognition, including secondary antibody fixation. Interestingly, the capability of recognition of CXCR4 positive cells by these immuno-LNCs persisted at full capacity for up to two days after formation (Supplemental Figure S1).

Considering the optimum bio-physical-chemical properties for CED injection reviewed by Allard *et al*. (to remain dynamic within the extracellular matrix

compartment, have a neutral or negative surface charge, and to present a steric coating to reduce non-specific binding, and finally to have a targeting moiety to recognize and adhere to a target cell), the ideal nanoparticles would be <100 nm in diameter (38). Hence, the radio-immuno-LNCs developed in the present work conforms with these requirements for optimum performance of CED injection.

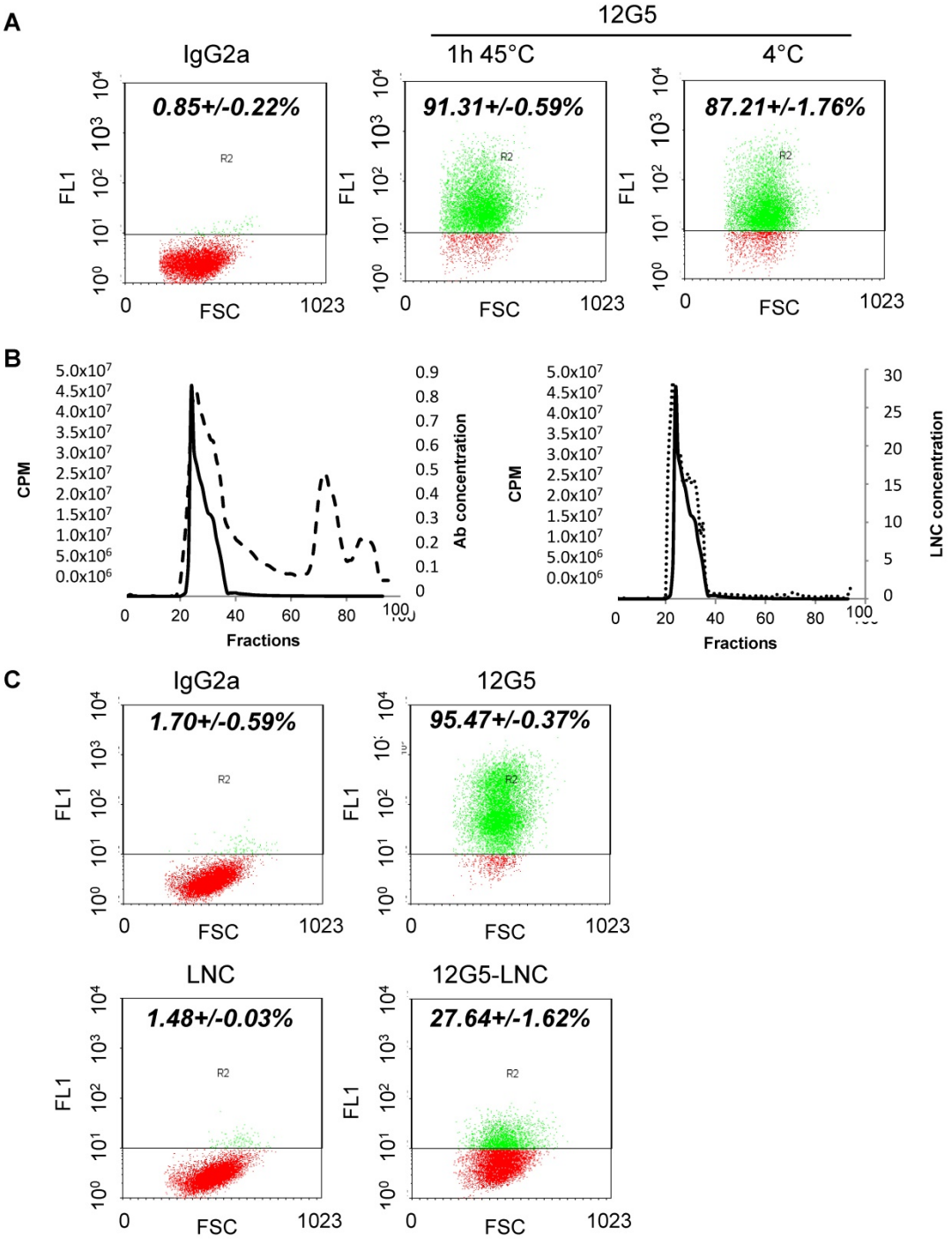

Figure 1. Synthesis of lipid nanocarriers and bio-physical-chemical characterization. A) Stability of recognition of the 12G5 antibody depending on temperature assessed by flow cytometry analysis. B) Validation of immuno-LNC synthesis. Thiolated antibodies (12G5 and IgG2a) were added to LNC^{188}Re or blank LNCs and incubated for 1 h at 45°C. Then, immuno-LNCs were purified on a sepharose column and positive fractions were concentrated. As represented on the left graph, micro-BCA assay was performed on each collected fraction to determine Ab concentration (dashed line) while gamma counting allowed measurement of the activity of each fraction (cpm, solid line). The right graph is representing LNC concentration determined by turbidimetric measurements (dotted line). C) Immunospecificity assay of free 12G5 antibody and 12G5-LNCs determined by flow cytometry.

Human GBM cells that constitutively overexpress the CXCR4 are tumorigenic and more aggressive *in vivo* than their wild type counterpart

In order to obtain a stable CXCR4-positive glioblastoma cell line, U87MG cells were transfected with an integrating non-replicative lentiviral vector coding for this receptor and the fluorophore RFP (red fluorescent protein) (Figure 2A). In our culture conditions, classical U87MG glioma cells were CXCR4-negative. After transfection, CXCR4 regular constitutive expression was checked by flow cytometry analysis. Figure 2B shows that, in cells transfected by the CXCR4 encoding lentiviral particle, 90% of cells are CXCR4-positive. Conversely, cells transfected by the control lentiviral construct are CXCR4-negative (Figure 2B).

To address their tumorigenic potential and orthotopic growth *in vivo*, U87MG CXCR4- and U87MG CXCR4+ cells were then implanted into the right striatum of SCID female mice. Tumor growth was monitored by MRI (Figure 2C). Images and calculated tumor volume showed that CXCR4-positive tumors were more invasive and grew faster than CXCR4-negative tumors. At day 9, CXCR4- tumors measured 0.9 mm^3 and did not grow in 8 days (0.6 mm^3 at day 17). Conversely, CXCR4+ tumors measured 4 mm^3 at day 9 and more than doubled in size in 8 days (10.2 mm^3 at day 17). Finally, the median survival (humane endpoint) of animals implanted with the two cell lines differed by about 5 days (30 versus 35 days) with an early clinical impact of the CXCR4 positive cells (Figure 2C).

In light of these results on tumor growth, which established tumor mass visible in a MRI from day 9 with the stable non-fluctuating CXCR4 positive glioblastoma cell line, it was decided that these mice would be further treated intracerebrally at the tumor site at day 12. To define the actual distribution of these CXCR4+/RFP+ tumor cells *in situ* and tumor characteristics at this stage, tumor tissue characteristics were determined at day 12 after U87MG CXCR4 positive tumor cell implantation by immunohistochemistry (Figure 2D). RFP expression (in red) established the expansion limit of the tumor mass while CXCR4 labeling demonstrated that most, if not all, tumor cells efficiently expressed CXCR4 at day 12. This result is essential with respect to our aim to target, at the locoregional level, a receptor associated with the target cells to eliminate them, and whose permanent expression is proved in all implanted RFP+ cells. Interestingly, CXCR4+/RFP+ tumors were highly labeled with the CD31 antibody, thus demonstrating a dense and homogenous vasculature of the tumor at day 12 (Figure 2D). Moreover, CD11b+ macrophages, which are also known to participate both in tumor growth and vasculogenesis, infiltrated the CXCR4+/RFP+ tumors at that stage, especially at the periphery of the tumor (Figure 2D).

Immuno-functionalization of ^{188}Re-loaded LNCs by a CXCR4-recognizing immunoglobulin improves their preclinical efficacy in CXCR4+ brain tumors after locoregional application through convection-enhanced delivery (CED)

The *in vivo* efficacy of internal radiation therapy with the functionalized 12G5-LNC^{188}Re was studied. Mice were treated with stereotactic injections of 2.7 MBq of LNC^{188}Re, 12G5-LNC^{188}Re or IgG2a-LNC^{188}Re or equivalent LNC concentration of non-radioactive nanocarriers, 12 days after U87MG CXCR4 positive cell implantation. These different treatments were administrated through CED at a flow of 0.5 µL/min for 20 min. In control animals, the median survival time was close to 36 days for both blank LNCs and saline solution, close to 39 days for IgG2a-LNCs and 12G5-LNCs, and close to 50 days for both LNC^{188}Re and IgG2a-LNC^{188}Re (Figure 3A and Table 2). There were no significant differences between the control groups ($p > 0.05$). Treatment with 12G5-LNC^{188}Re was associated with a 50% increase in median survival time (IMST) compared to non-radioactive treatments, with two animals surviving more than 100 days (long survivors). MRI follow-up with representative images, Figure 3B, corroborated this observation. Tumors were present in each group at the beginning of the experiment. Tumors regressed or totally disappeared when the animals were treated with 12G5-LNC^{188}Re, IgG2a-LNC^{188}Re and LNC^{188}Re with various times to progression. Mice treated with LNC^{188}Re presented a new visible tumor mass as early as 65 days, animals treated with IgG2a-LNC^{188}Re relapsed from 85 days on and those treated with 12G5-LNC^{188}Re from 100 days on (Figure 3B). Thus, CED infusion of 12G5-LNC^{188}Re was the most effective treatment with the longest measured time to progression. Nevertheless, there were no significant differences between the 12G5-LNC^{188}Re treated group and other rhenium treated groups (IgG2a-LNC^{188}Re and LNC^{188}Re) and only 12G5-LNC^{188}Re treated mice had a significant survival benefit compared to non-radiated animals (significant difference compared to 12G5-LNCs and IgG2a-LNCs and very significant difference compared to saline solution and blank LNCs) (Figure 3A and Table 2).

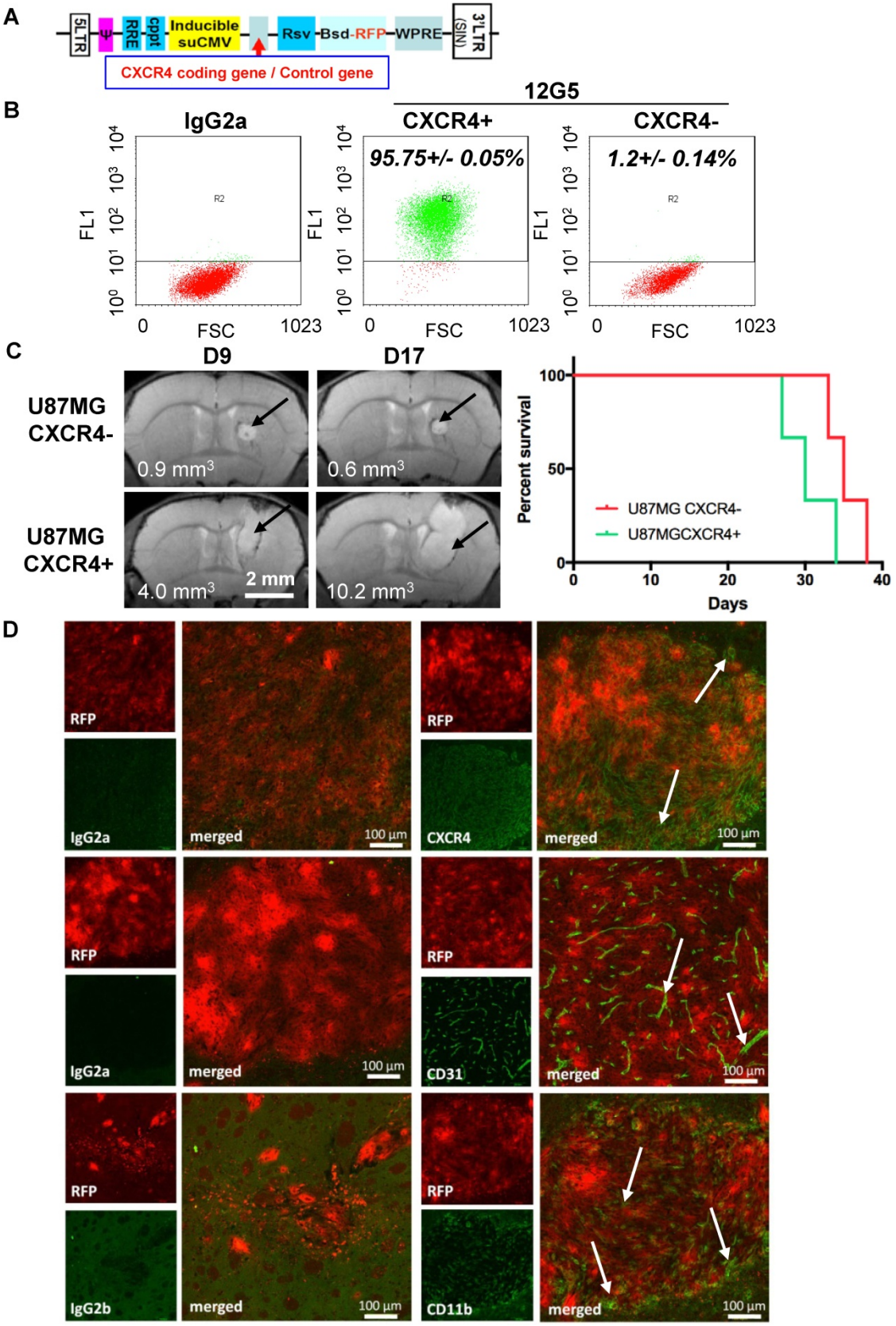

Figure 2. Orthotopic *in vivo* implantation of CXCR4 overexpressing cells reveals their tumorigenic potential and their intrinsic aggressiveness. A) Schematic representation of lentivirus coding for CXCR4 or a control gene. B) Cytometry analysis performed on U87MG transfected cells. The 12G5 antibody efficiently labeled U87MG CXCR4+ cells but not U87MG negative cells, transfected with the control lentivirus. C) Representative MRI performed at day 9 and day 17 after implantation of U87 CXCR4- cells and U87 CXCR4+ cells (arrows indicate tumor tissue) with resulting apparent tumor volumes and corresponding Kaplan-Meier curves. D) Immunohistochemistry analysis of U87 CXCR4+ tumors 12 days after implantation. CXCR4, CD31, CD11b and corresponding isotype control labeling appears in green (arrows) with RFP in red.

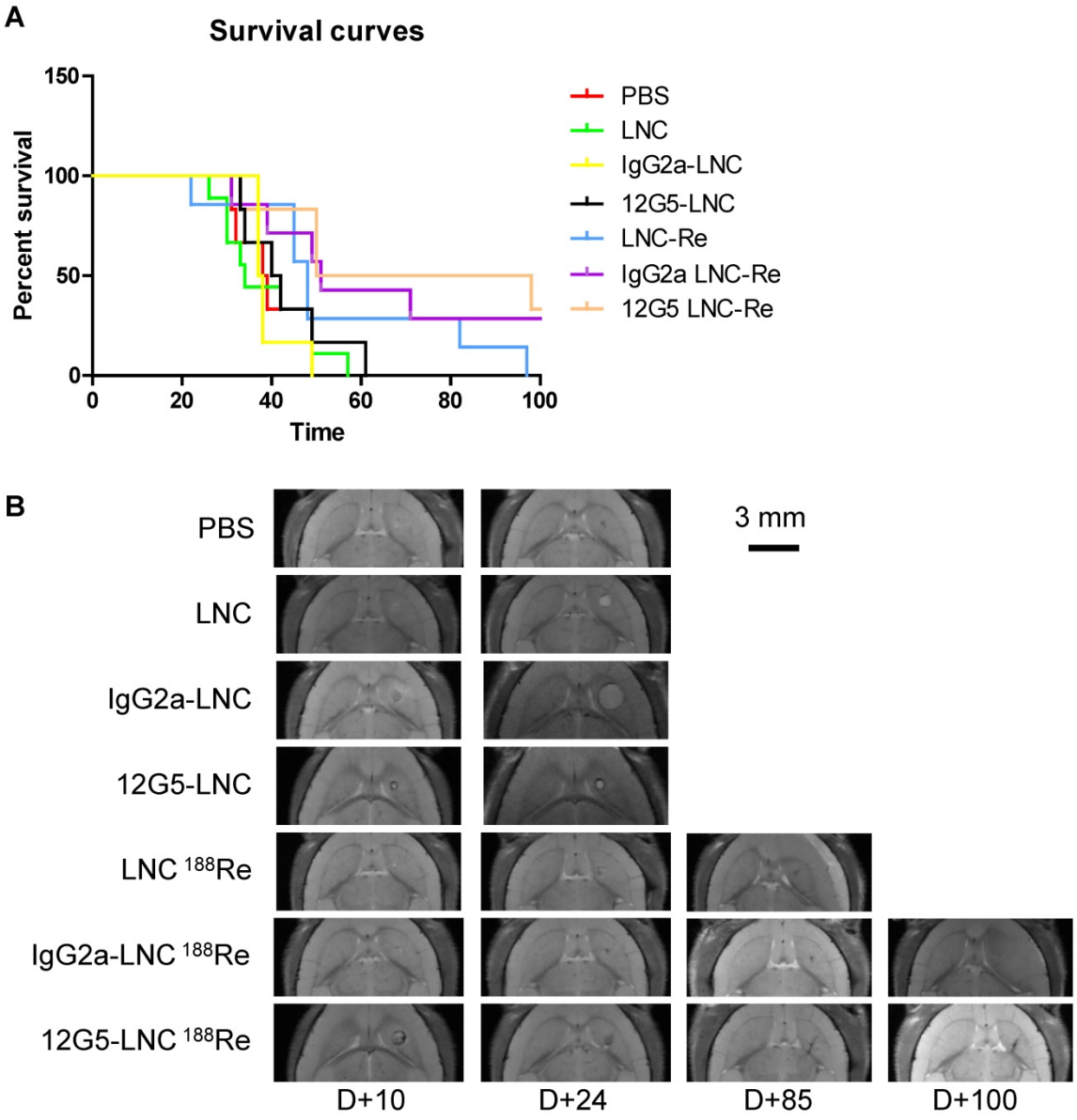

Figure 3. Immuno-functionalization of ^{188}Re-loaded lipid nanocapsules by a CXCR4-recognizing immunoglobulin reveals their preclinical efficacy after single infusion through convection-enhanced delivery into CXCR4-positive brain tumors. A) Kaplan Meier curves. B) MRI follow-up of mice treated with saline solution (PBS), blank LNC, immuno-LNCs (12G5-LNCs and IgG2a-LNCs) and internal radiation therapies (LNC^{188}Re, IgG2a-LNC^{188}Re and 12G5-LNC^{188}Re).

Table 2. Statistical analysis of mice survival performed with Log rank test (* $p < 0.05$; ** $p < 0.001$)

	PBS N=6	LNC N=9	IgG2a-LNC N=6	12G5-LNC N=6	^{188}ReLNC N=7	IgG2a^{188}ReLNC N=6	12G5^{188}ReLNC N=7
Median survival (days)	38.5**	34**	41*	37.5*	48	51	74

Overall, we broadened the preclinical impact of ^{188}Re-loaded-LNCs, which was a function of the structure of the LNC (immuno-LNCs versus classical LNCs) and might be related to their capability of recognition of the CXCR4 receptor favoring specific tissue containment (cf. paragraph "Immuno-functionalization of lipid nanocapsules by a CXCR4 recognizing immunoglobulin had a significant impact on their *in situ* distribution and containment in brain areas holding CXCR4-targeted tumor cells". These pre-clinical effects may indeed be independent of a functional block of SDF-1 pathway caused by the 12G5 antibody combined with the nanocarrier system, as supported by *in vitro* exploration of downstream signals such as Akt phosphorylation on serine-473, which was not significantly affected by co-treatment by SDF-1 combined with 12G5-LNCs, while expression of total Akt remains stable (Supplemental Figure S2). 12G5-LNCs even slightly activated the pathway.

Treatment with 12G5-LNC^{188}Re had a significant impact on the phenotype of radioresistant tumors

In order to define the locoregional effects of CED treatment on tumor phenotype with ^{188}Re-loaded-LNCs versus unloaded-LNCs, immunohistological investigations were performed at 7 days post CED corresponding to 19 days post cell implantation. Analysis of CD31, CD11b MMP9 and Ki67 expression in tumor bearing brains revealed no major modifications of tumor vascularization, invasion macrophage infiltration, or cell proliferation in the presence of ^{188}Re-loaded-LNCs, at this stage of analysis (data not shown).

To further investigate the histological profile and phenotype of tumors that resisted the radiotherapeutic protocols, an immunohistological analysis was also performed by considering the humane endpoint in animals that would have died from their tumor. Animals were sacrificed when they lost 10% of their original weight. As for the treatment day, tumor vasculature and CD11b+ macrophage infiltration were evaluated and tumor cells were red (RFP+, CXCR4+) (Figure 4). No significant differences between tumor vasculature were observed whatever the treatment, only the brains of 12G5-LNC^{188}Re and IgG2a-LNC^{188}Re treated mice presented less CD31 labeling, and the tumors in 12G5-LNC^{188}Re treated mice appeared to be hypovascularized compared to other tumors. Interestingly, CD11b+ labeling was inversely proportional to tumor vasculature. Indeed, there was a high CD11b+ infiltrate in the brains of 12G5-LNC^{188}Re treated mice, much higher than with the other treatments. Nevertheless, tumor bearing brains from LNC^{188}Re and IgG2a-LNC^{188}Re treated mice also presented a higher CD11b+ infiltrate. In order to better understand the significance of this increase in myelomonocytic lineage cells in tumors treated with nanovectorised radiation therapy, and although we are in a non-immune paradigm (SCID mouse), macrophage polarization phenotype, which represents a useful simplification for the demonstration of their plasticity and adaption to tumor development and treatment, was investigated (39). Immunocharacterization of the continuum existing between the CD68+/NOSII+ M1 phenotype cells (notably associated with tumor destruction and tissue damage) and the CD68+/Arg1+ M2 phenotype (usually associated with tumor promotion and tissue remodeling) performed on adjacent brain cryosections demonstrates that CD68 positive brain areas in radiation treated animals (not in controls) were expressing Arg1 and NOSII. However, those two biomarkers where topographically expressed in clear distinct zones of the tumor with NOSII from the inside to the external part of the tumor while Arg1 was exclusively present in the peripheral part of the tumor (Figure 4D).

Immuno-functionalization of lipid nanocapsules by a CXCR4 recognizing immunoglobulin had a significant impact on their *in situ* distribution and containment in brain areas holding CXCR4-targeted tumor cells

Prior to defining preferential staining of LNCs in the cerebral tissue of tumor bearing mice, intrinsic fluorescence of parenchyma containing CXCR4+(RFP+) cells and CXCR4-(RFP-) cells (chimeric tumor) were characterized using spectral imaging. The spectral imaging method (35) is described in the experimental section and illustrated in Figure 5. Briefly, zones of brain sections were selected at the interface between the tumor and peritumoral parenchyma tissue (Figure 5A) and the spectral images of these zones were generated. First, full fluorescence spectra in the range of 500-800 nm (Figure 5C) were recorded at each point scanned with a 488 nm laser. Second, spectral analysis of the brain spectra allowed us to determine three characteristic spectra (Figure 5D): a red spectrum corresponding to RFP+ cells (emission maximum at 590 nm), a blue spectrum for tumor tissue without RFP (main emission maximum at 700 nm) and a green spectrum for peritumoral cerebral tissue (main emission maximum at 555 nm). Third, each spectrum was then fitted with a proportional contribution of the characteristic spectra and the fitting coefficients served to generate the spectral maps corresponding to the topographic distribution of these spectra, i.e., RFP, tumoral and peritumoral regions of the samples (see Figure 5F-H and their merge in Figure 5B). As can be seen by comparing the total fluorescence intensity map (Figure 5E) with the spectral map of RFP (Figure 5F), spectral imaging allows really specific localization of the RFP+ cells (CXCR4 positive cells). These cells are distributed on the periphery of the tumoral/peritumoral tissues.

Next, a similar approach was applied to study the distribution of two kinds of DiD-loaded immuno-LNCs (IgG2a-DiD-LNCs or 12G5-DiD-LNCs) after their injection into the brain (Figure 6). For this purpose, the sample spectra at each point were fitted with four characteristic spectra (Figure 6A): the three spectra described above and an additional one (magenta curve) found in the brain tissues close to the immuno-DiD-LNCs injection site and recognized due to a characteristic DiD fluorescence maximum at 670 nm. The respective maps of RFP, DiD and their merge with tumoral

(blue) and peritumoral (green) zones as well as their overlay with the white light images of the tissue samples are shown in Figure 6B. Finally, the co-localization of RFP with DiD fluorescence was calculated in these specific zones and the statistical summary is represented by the histogram in Figure 6C.

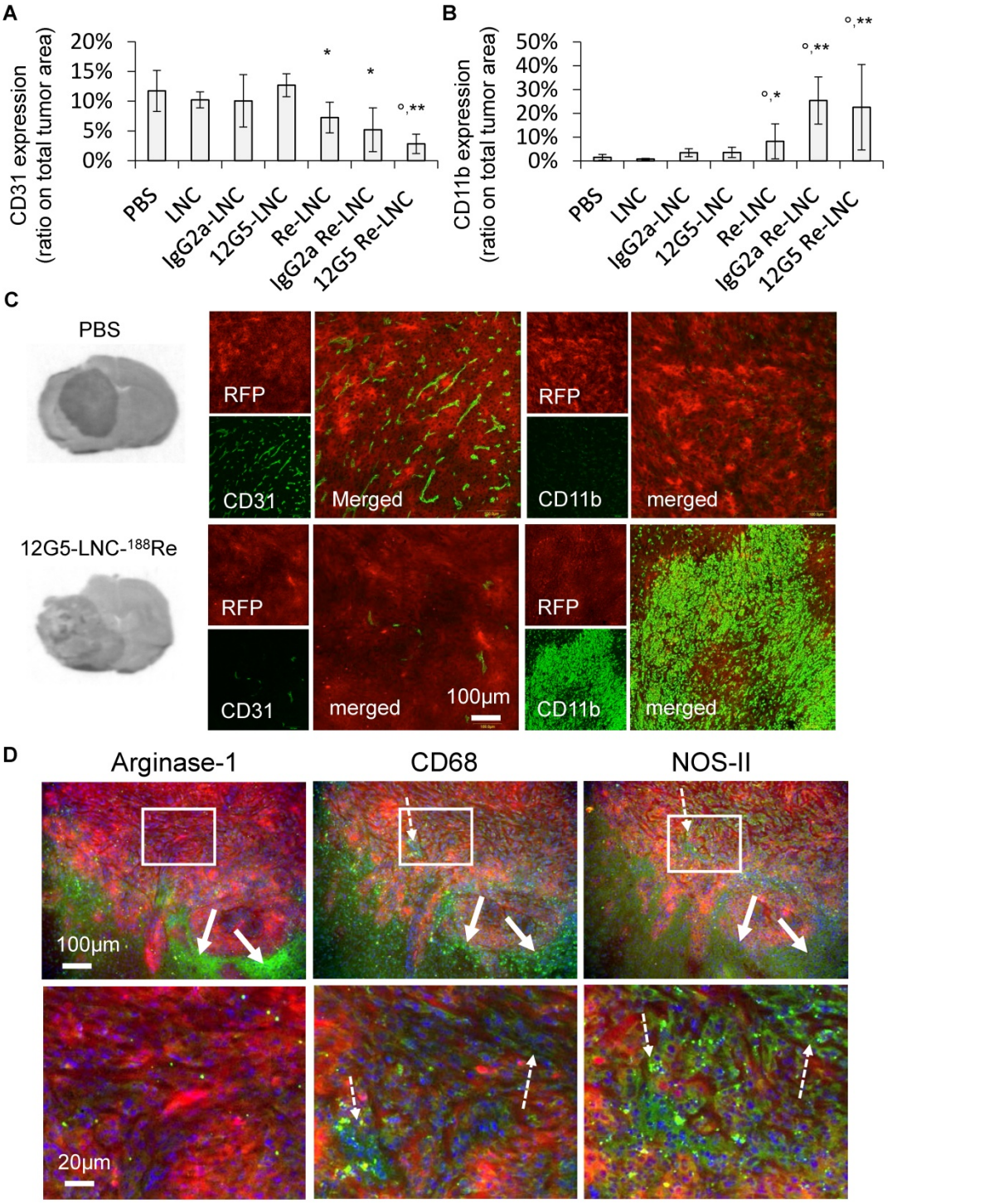

Figure 4. Immunohistochemical analysis of brain tumors at end point reveals hypovascularization and stimulation of the recruitment of bone marrow derived CD11b-positive cells in 12G5-LNC^{188}Re treated animals. A) Quantification of CD31 expression from tumor bearing mice treated with saline solution (PBS), blank LNCs, IgG2a-LNCs, 12G5-LNCs, LNC^{188}Re, IgG2a-LNC^{188}Re, 12G5-LNC^{188}Re. B) Quantification of CD11b expression from tumor bearing mice treated with saline solution (PBS), blank LNCs, IgG2a-LNCs, 12G5-LNCs, LNC^{188}Re, IgG2a-LNC^{188}Re, 12G5-LNC^{188}Re. C) Representative images of brain sections for the 12G5-LNC^{188}Re situation as compared with the PBS situation, showing hypovascularized and more CD11b-positive cells infiltrated in 12G5-LNC^{188}Re-treated tumors. RFP, red fluorescent protein, appears in red with CD31 or CD11b staining in green. On the left: black and white images of hematein eosin staining of brain sections. *p*-values: **p*<0.05, ***p*<0.01, comparisons with the PBS control situation; °*p*<0.05, comparisons with the Re-LNCs situation. D) Immunohistochemical analysis of the expression of CD68, NOSII and Arg1 on adjacent tumor brain cryosections; representative images of brain sections for the 12G5-LNC^{188}Re situation. Note the exclusive Arg1 staining at the peripheral part of the tumor (arrows) while NOSII correspond with all the tumor area labeled by CD68 (arrows and squares). Bottom panels are enlargements of upper rectangles.

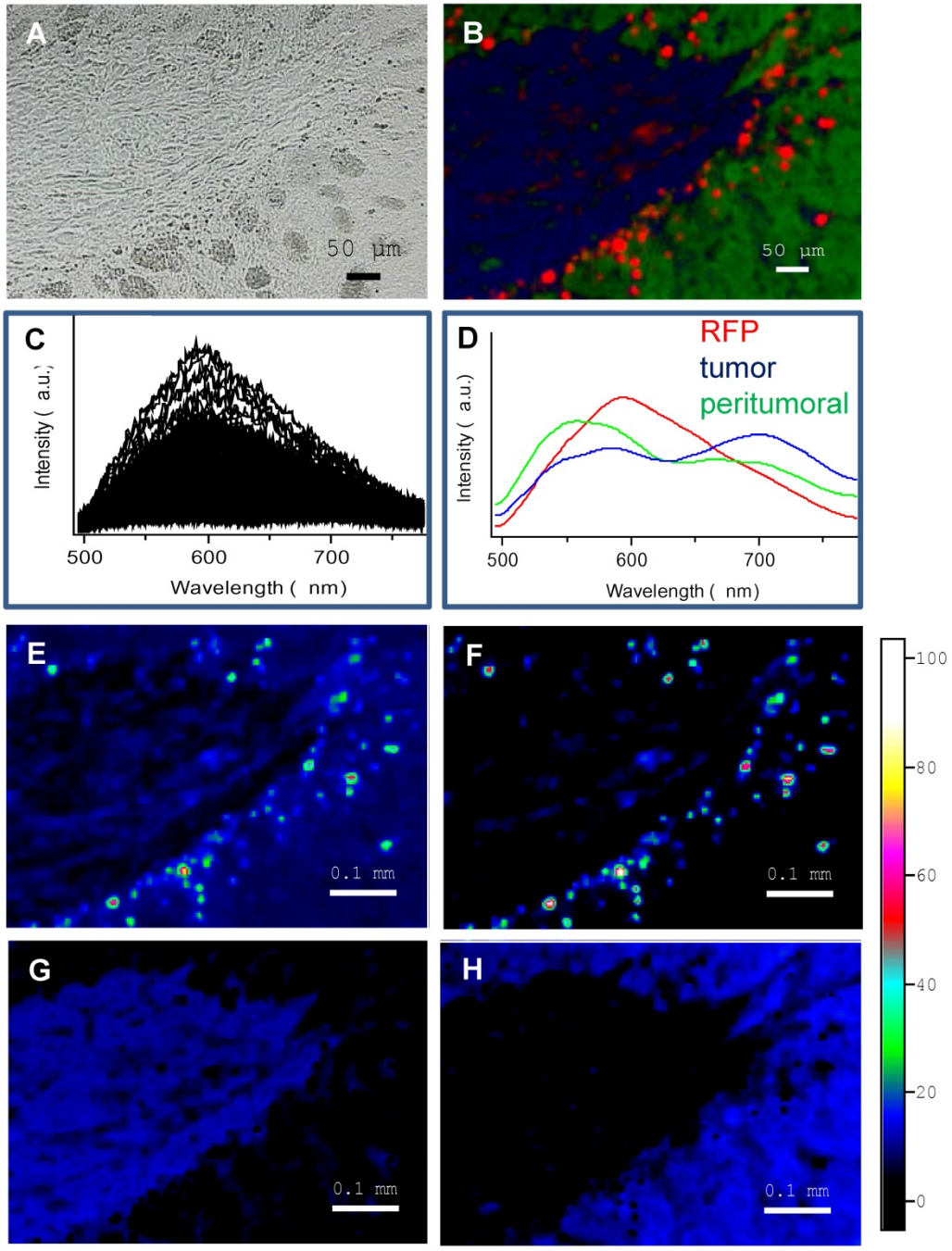

Figure 5. Fluorescence spectral imaging analysis emphasized the infiltrative nature of CXCR4 positive cells. A) White light image of the tissue. B) Merge of three spectral maps shown with pseudocolors corresponding to the three model spectra from D (note the RFP-CXCR4-positive cell migratory front (in red) throughout the tumor margin (from the blue to the green area)). C) Overlay of fluorescence spectra recorded from a scanned region of the brain tissue. D) Model fluorescence spectra of RFP (red), tumor autofluorescence (blue) and autofluorescence of peritumoral parenchyma tissue (green). E) Total fluorescence intensity map. F-H) spectral maps of RFP (F), tumor (G) and peritumoral parenchyma tissue (H). The relative intensity of the encoding scale (from cold to hot) of the maps E-H is shown on the right.

As can be seen in Figure 6, when the brain was treated with immuno-DiD-LNCs, the co-localization of with the CXCR4 positive cells was more pronounced (48.0%) for 12G5-DiD-LNC nanocarriers than for IgG2a-DiD-LNCs (9.6%). Thus, 12G5-DiD-LNCs appeared to be more efficiently retained in the tissue that expressed its receptor CXCR4 than IgG2a-DiD-LNCs.

Discussion – Conclusion

The aim of this study was to investigate the preclinical feasibility and benefit of a functionalization of LNCs for specific cellular targeting in the context of vectorized internal radiation therapy. We demonstrate that 12G5-LNC^{188}Re single infusion treatment by CED

resulted in a major preclinical improvement in the median survival time accompanied by locoregional effects on tumor development including hypovascularization and stimulation of the recruitment of bone marrow derived CD11b-positive cells. Interestingly, thorough analysis by spectral imaging in a chimeric U87MG GBM model containing CXCR4-positive/RFP-positive- and CXCR4-negative/RFP-negative-GBM cells revealed greater confinement of DiD-labeled 12G5-LNCs than control IgG2a-LNCs in RFP compartments. Regarding the additional functionality of the nanocarrier several aspects have to be emphasized: firstly, the retention of rhenium within the brain organ due to the nanoparticle (14) and secondly, the interest of this new-generation of custom-made immunonanocarriers constituting a radiopharmaceutical of particulate type as opposed to a molecular one (free antibodies or peptides) (40). Hence, the outcome (distribution, efficacy, activity gradient) of the radionuclide used is here tightly associated to the nano-bio interface properties of the newly developed nanosystems.

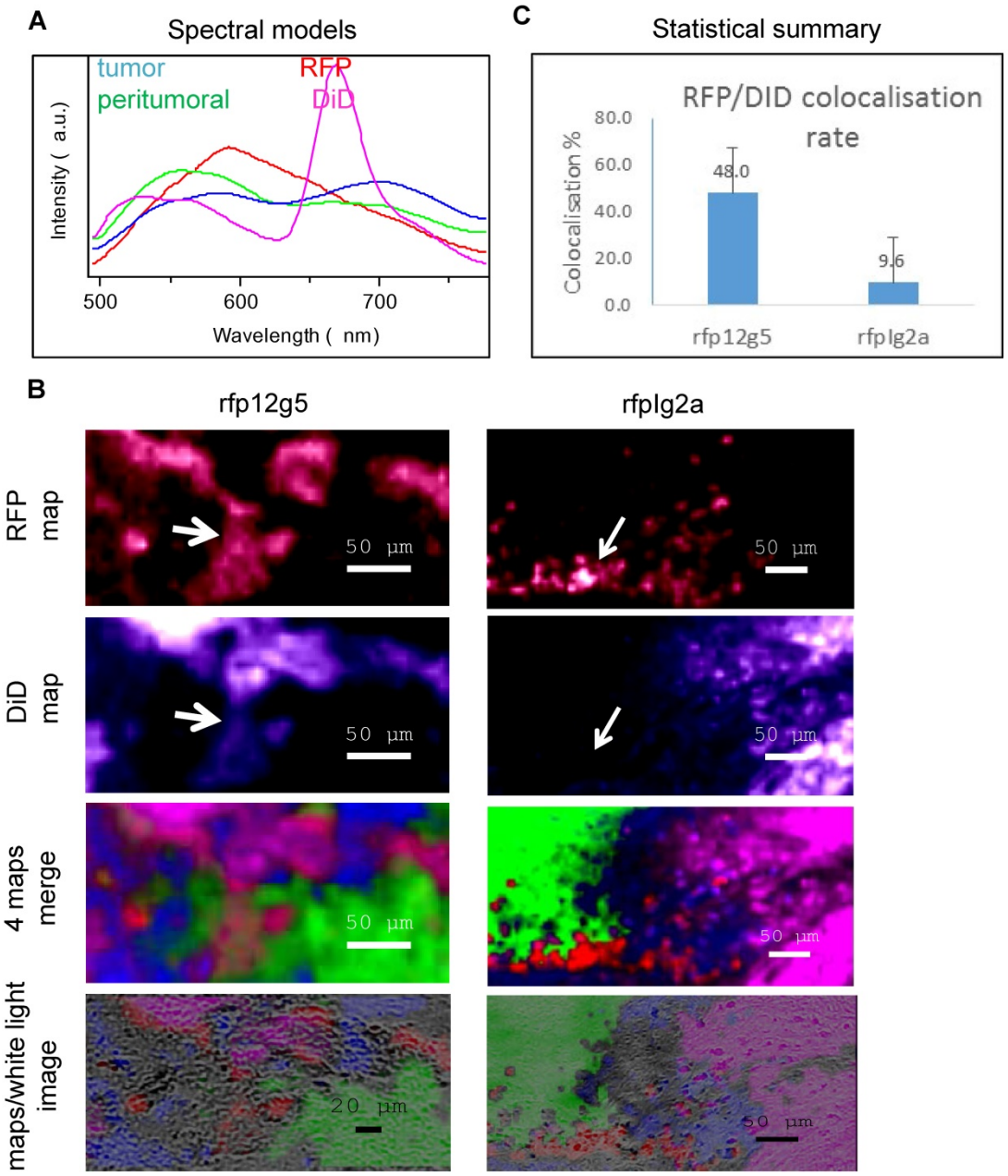

Figure 6. Spectral characterization of immuno-DiD-LNCs (12G5-DiD-LNCs and IgG2a-DiD-LNCs) distribution within the brain parenchyma of tumor bearing mice established a preferential containment of CXCR4-immuno-functionalized lipid nanocapsules in brain areas holding CXCR4-targeted tumor cells. A) characteristic spectra used to generate the spectral maps: three from Figure 5 and the fourth (magenta) for DiD-stained tissues. B) From top to bottom: spectral maps of the fluorescence of RFP (red); DiD (magenta); merge of the 4 spectral maps: RFP (red), DiD (magenta), tumor (blue) and peritumoral (green); the map overlay on the white light image of the scanned brain tissue region. Note the strong co-localization for RFP and DiD for the 12G5 situation (rfp12g5) in comparison to the IgG2a situation (rfpIg2a) (cf. matching white arrows). C) Statistical summary of calculated co-localization of RFP with DiD fluorescence.

On the preclinical benefit of 12G5-LNC^{188}Re in an orthotopic CXCR4-U87MG human to mouse model of glioblastoma

LNC^{188}Re indeed had a greater biological impact when combined with the 12G5 antibody. Although this result was the working hypothesis, it implied several phenomena associated with the behavior of the radiolabeled nanocarriers. Among those, only a small fraction of the nanocarriers used is effectively radiolabeled, making it possible for blank-LNCs to compete with ^{188}Re-loaded LNCs in the same injected suspension. The fact that the CXCR4 targeting increases the impact of ^{188}Re-loaded LNCs could be ascribed to the rapid turnover of the CXCR4 receptor in the parenchyma of the brain tumor (41). This could also be linked with the integrity of the nanocarrier and the half-life of the radionuclide, another possibility being that surface modification of the immune-nanocarrier when loaded with ^{188}Re complex confers an advantage of recognition of the 12G5 immunoglobulin. In the present study, we found that 12G5-immunonanocarriers recognized the CXCR4 with a lower apparent yield as compared with the free 12G5 (Figure 1C). Finally, 12G5 immunolabeling of LNCs may have resulted in the recognition of many distinct cell types, not only tumor cells constitutively expressing the receptor but also other cells associated with tumor development such as monocyte/macrophage CD11b+ (29), microglial cells (42) vascular endothelium (43), glioma/neuronal progenitor cells (44).

In line with this hypothesis, tumors that developed after the 12G5-LNC^{188}Re treatment presented distinct phenotypes with more infiltrating macrophages and lower vasculature at the end point, a phenomenon that may have resulted from direct effects on tumor associated cells but also from indirect effects on CXCR4-U87MG cells that can corrupt their micro-environment. As such, radiation impact on invasion (45), with CXCR4-positive cells located at the front of tumor progression in our chimeric model (Figure 5B), and hypoxia might be involved (46). Interestingly, analysis of macrophage pools present in tumors induced by loco-regional irradiation supports the cohabitation of the two extremes of the M1/M2 continuum as not randomly distributed but organized with M2-type cells on the colonization front of the tumor, supporting the idea that that these cells participate in the tumor expansion. In contrast, the M1 cell types, classically not found in GBM tumors (47), were found in large numbers within the cancerous parenchyma, an indication of the response to treatment that holds much clinical potential for immunonanoparticle-based radiotherapy. Hence, specific investigations of the role of these contingents and their combined polarization/repolarization (48,49) deserve to be further performed, also in immune models, in order to improve nanovectorized irradiation schemes (dose fractionation, synergy with chemotherapy) with regard to local recurrences. Correlations with CXCR4 fluctuations and molecular genetics in patient-derived GBM cells would also be of key interest.

On the region-specific confinement of 12G5-LNC^{188}Re within the brain tumor parenchyma of orthotopic CXCR4-U87MG human to mouse model of glioblastoma

A major result of this study is validation of the hypothesis that immuno-nanocarriers effectively recognize CXCR4-positive cells *in vivo*. Thorough analysis using a cutting edge spectral imaging technology in a chimeric U87MG GBM model containing CXCR4-positive/red fluorescent protein (RFP)-positive and CXCR4-negative/RFP-negative-GBM cells revealed greater confinement of DiD-labeled 12G5-LNCs than control IgG2a-DiD-LNCs in RFP compartments. This is an advance over previous work demonstrating the *in vitro* activity of OX26-immuno-LNC targeting the transferrin receptor on rat lymphoblast cells (50) or of AC133-immuno-LNC targeting the CD133 on human epithelial colorectal adenocarcinoma cells (33). In their work, Bourseau *et al.* engrafted ~30 mAbs on LNCs (with method 2 used in the present study) whereas in our study, we obtained ~10 mAbs on the surface of the LNC. The difference in the number of mAbs engrafted on the LNCs could be attributed to the different amounts of thiolated groups on the Fc fragments of AC133 and 12G5. Nevertheless, this strongly implies added functionality for the third generation nanocarrier, not only stealth properties but also a functional targeting moiety while retaining nanoscale size (~75 nm) with homogeneous populations (PDI ~0.2).

In our study, CED was used to infuse the 12G5-immuno-nanocarriers. Previously, Vanpouille *et al*. highlighted the usefulness of rhenium-188 encapsulation by showing that ^{188}Re-loaded-LNCs maintained high levels of radiopharmaceuticals in the brain (14). Thus, 96 h after injection, only 4% and 65% of, respectively, LNC^{188}Re and the solution of Re-perrhenate (ReO_4) injected dose were eliminated in urine and feces. These authors also revealed the importance of the administration route in the activity gradient. Although biodistribution was similar using simple (SI) or CED injections, the distribution within the brain tissue revealed LNC^{188}Re spread to be greater with CED than with SI administration and

radioactivity content to be more concentrated by the SI injection than CED. Thus, like others before (51), Vanpouille *et al*. demonstrated that CED injection provides a much larger volume of distribution than is achievable by diffusion and rhenium-188 encapsulation reduces radiopharmaceutical clearance.

In the present work, we showed cellular confinement of the vector in the tumor brain tissue. Spectral imaging analysis showed that 12G5-DiD-LNCs co-localized with RFP+ zones (CXCR4+) more efficiently than IgG2a-DiD-LNC. Thus, 12G5-LNCs appeared to be retained in the CXCR4+ zone in the tumor. This effect did not depend on the presence of immunoglobulin on the surface of the LNC, because IgG2a-DiD-LNCs had a weak co-localization with RFP+ (CXCR4+) zones, but depended on the presence of 12G5. This vectorized radiotherapy can be linked with the concept of dose-painting (52), which consists of heterogeneous radiation delivery within the tumor targeting the radioresistant zone defined by functional imaging. In this concept, the tumor is not considered as a homogeneous mass composed of similar cells but rather as a complex model with different cell subtypes with different radioresistances and aggressiveness profiles (53). Radioresistance is due to tumor factors like cancer stem-cells, intrinsic radioresistance or proliferation capacity and to factors linked to the microenvironment like hypoxia or immune cells (54). After identification of high metabolism zones, proliferation markers or hypoxia by imaging, this technique would allow specific targeting of cells involved in radioresistance. A clinical trial on relapsed GBM patients demonstrated that increasing radiation doses targeting active metabolic zones improved patient survival (55). Another study on relapsed glioblastoma showed the potential advantage of radiation of ^{11}C-methionine or ^{123}I-alpha-methyl-tyrosine attracted zones for patient survival compared to a non-dose-painting treated group (56). In a recent review, Lemee *et al*. recalled that intratumoral heterogeneity is not only limited to the tumor itself, but also involves the peritumoral brain zone (PBZ), which has specific properties that contribute to GBM heterogeneity (57) and 90% of recurrences occur in this area (58). Thus, the nanovectors we created in this study could be a way of concentrating radiation damage in a targeted zone, particularly in areas where surgical resection is impossible and external beam radiation is difficult to focus. They distinguished from particulate systems allowing increasing the deposition of dose obtained after external radiotherapy (59,60) because of a sustained intrinsic action and, also, from free-radiolabeled molecules or complexes (40,61) due to specific local elimination and stability properties of the object of radiotherapy (62).

On the impact of 12G5-LNC^{188}Re and CXCR4 signaling

Our study established that 12G5-LNCs are confined in the vicinity of CXCR4 positive cells but that *in vitro* the mAb 12G5 failed to exert a blocking activity while present on the surface of the nanoparticles (Supplemental Figure S2).

Although blocking the CXCR4 receptor *in vivo* through the 12G5-LNC^{188}Re is a possibility, it seems clear that their preclinical benefit is mainly due to their higher retention in a CXCR4 positive tumor tissue compared with other nanocarriers, and they can thus irradiate this tissue more efficiently. Radiation induces hypoxia due to loss of endothelial cells (EC). After radiation, the irradiated tumor gradually loses vasculature, thereby becoming increasingly hypoxic and up-regulating hypoxia inducible factor-1 (HIF-1) (30). Then, SDF-1 functions as a hypoxia-inducible gene through the action of the transcription factor HIF-1. Elevated SDF-1 levels lead to accumulation of CXCR4-expressing monocytes/macrophages CD11b+, the precursors of tumor-associated macrophages (TAMs) in the irradiated tissue (29,30). Thus, the increase in TAMs after irradiation could be due to increased tumor HIF-1 levels since HIF inhibition completely abolished their recruitment (63). Given the M1 and M2 phenotypes observed in the treated tumors, a selective recruitment or down-regulation of the expression of M2 genes are most likely involved in the polarization of these cells *in situ* notably at the center of the tumor (M1 phenotype), which may be part of the beneficial impact of the nanovectorized radiation therapy (39).

Thus, it is possible that radiation induced by 12G5-LNC^{188}Re was higher than that induced by other rhenium treatments due to its stronger persistence within the CXCR4+ tumor tissue, and induced a higher hypoxia than LNC^{188}Re and IgG2a-LNC^{188}Re. After treatment, 12G5-LNC^{188}Re-treated tumors became very hypoxic leading to their regression, and made them undetectable by MRI follow-up. Initially, tumor progression was contained but then hypoxia induced CD11b+ monocyte/macrophage migration to the tumor site stimulated tumor progression.

As the present study only monitored animal survival until 100 days, we cannot know if tumors regrow after this date. Nevertheless, it is possible that a single dose 12G5-LNC^{188}Re was not sufficient to block CD11b+ dependent vasculogenesis and hence cannot be a curative therapy.

Another explanation is possible. With the 12G5 antibody, we only inhibited the interaction between

SDF-1 and one of its receptors, CXCR4. However, SDF-1 has a second receptor, CXCR7, implicated in endothelial cell migration (64,65), that is present on tumor vasculature (64) and is potentially also able to activate vasculogenesis. In a recent study, Walters *et al.* used a specific inhibitor of CXCR7, CCX771 in the intracranial U251 GBM mouse model. As for CXCR4, they found that the CXCR7 inhibitor did not affect the growth or survival of the tumor in rodents that did not receive local brain irradiation, but significantly increased the delay in tumor growth and the survival of the animals that had received local brain irradiation (66,67). Thus, the involvement of both CXCR4 and CXCR7 suggests that SDF-1 could be the master regulator of vasculogenesis. Inhibition of SDF-1 interaction with both CXCR4 and CXCR7 with specific inhibitors or a SDF-1 inhibitor could enhance the impact on tumor vasculogenesis and radiosensitivity.

Conclusion

Overall, our findings strongly support the hypothesis that the use and optimization of intracerebral active targeting of nanocarriers loaded with radiopharmaceuticals may have considerable benefits in human clinical trials. It would thus be of interest to further explore these locoregional capacities in comparison with those of free radiolabeled-antibodies and the impact of other theranostic radiopharmaceuticals with distinct radiochemical properties based on the use of beta- (^{90}Y, ^{177}Lu) or alpha- (^{211}At) particle emitting radionuclides. As such a recent first-in-human experiment with CXCR4-targeted therapy using ^{90}Y- and ^{177}Lu-pentixather appears promising in multiple myeloma (68). In addition, as the importance of the immune system in eradicating tumor mass has already been demonstrated (14), relations with the immune system, notably with dendritic cells, while confining nanocarriers in specific brain-tumor areas, would be of major interest.

Abbreviations

BBB: blood-brain barrier; BSA: bovine serum albumin; CED: convection-enhancement delivery; GBM: glioblastoma; GSC: glioma stem-like cell; LNC: lipid nanocapsule; LNC^{188}Re: rhenium-188 loaded lipid nanocapsule; mAb: monoclonal antibody; MS: median survival; NOSII: inducible type-2 nitric oxide synthase; PBS: phosphate buffer saline; PBZ: peritumoral brain zone; PDI: polydispersity index; RARE: rapid acquisition with relaxation enhancement; RFP: red fluorescent protein; RT: room temperature; SSS: lipophilic thiobenzoate complexes; TAM: tumor-associated macrophages; TE: echo time; TR: repetition time.

Supplementary Material

Supplemental materials are informative on the time storage stability of the newly developed immunonanoparticles before use and on their interaction with the SDF-1 signaling pathway. Supplemental Figure S1 present an analysis of the immunoreactivity of free 12G5 antibody and 12G5-LNCs as a function of time after storage at 4°C determined by flow cytometry on U87MG CXCR4+ cells. Supplemental Figure S2 represent a Western blot analysis of the phosphorylation of Akt in U87MG CXCR4+ cells 16 hours after stimulation by SDF-1 at 25nM depending from the presence of LNC formulations (12G5-LNCs, IgG2a-LNCs and LNCs) or not (PBS). http://www.thno.org/v07p4517s1.pdf

Acknowledgements

We would like to thank the Federative Structure of Research Health of Angers, SFR 4208 ICAT, Catherine Guillet from the "*Service Commun de Cytométrie et d'Analyses Nucléotidiques*" (SCCAN, Angers, France), Rodolphe Perrot from the "*Service Commun d'Imageries et d'Analyses Microscopiques*" (SCIAM, Angers, France), Pierre Legras et Jérôme Roux from the "*Service Commun d'Animalerie hospital-universitaire*" (SCCAN, Angers, France) and Laurent Lemaire from the "*Plateforme de Radiobiologie et d'Imageries Expérimentales*" (PRIMEX, Angers, France). We also thank Philippe Moullier and Véronique Blouin from INSERM U1089 (Nantes, France), Damien Autret and Magali Edouard from the "*Institut de Cancérologie de l'Ouest*" (ICO, Angers, France) and Ellyn Renou from Team-17 of INSERM U1232 for useful technical support. We are grateful to James Hoxie from the University of Pennsylvania (Philadelphia, USA) who provided the 12G5 hybridoma and Jeremy Riou from INSERM U1066 (Angers, France) for beneficial advices on statistics.

Funding

This work was supported by "La Région Pays-de-la-Loire" through the Nuclear Technology for Health project (NucSan), by the "Institut National de la Santé et de la Recherche Médicale" (INSERM), by "La Ligue Nationale Contre le Cancer" through an "Equipe Labellisée 2012" grant and by the "Axe Vectorisation and Radiothérapies of the Cancéropôle Grand-Ouest". Delphine Séhédic was a Ph.D. student from the NucSan project and received a fellowship from "La Région Pays-de-la-Loire". N.L., F.H., F.D. and E.G. are also member of the LabEx IRON "Innovative Radiopharmaceuticals in Oncology and Neurology" as part of the French government

"Investissements d'Avenir" program. The presented work is also related to the PL-BIO 2014-2020 INCA (Institut National du Cancer) project MARENGO - "MicroRNA agonist and antagonist Nanomedicines for GliOblastoma treatment: from molecular programmation to preclinical validation", to the ANR (French National Research Agency) program RADIOHEAD "Nanocapsules for Selective Internal RadioTherapy of glioblastoma, and to the "Région Pays-de-la-Loire" project IRAD" Pre-clinical validation of an innovative Internal RADiotherapy of glioma in a large spontaneous animal model". C.Lo., and C.Le. were posdoctoral fellows from Inca and Fondation ARC, respectively.

Author contributions

D.S., I.C., C.T., A.G., C.Lo., S.A., C.Le., N.L., E.G. performed the experiments. D.S., I.C., D.W., F.H., F.D, E.G. contributed to the design and interpreted the data, D.S. and E.G. drafted the manuscript. F.D. and E.G. obtained the funding.

Competing Interests

The authors have declared that no competing interest exists.

References

1. Bondy ML, Scheurer ME, Malmer B, Barnholtz-Sloan JS, Davis FG, Il'yasova D, et al. Brain tumor epidemiology: consensus from the Brain Tumor Epidemiology Consortium. Cancer. 2008;113(7 Suppl):1953–68.
2. Stupp R, Mason WP, van den Bent MJ, Weller M, Fisher B, Taphoorn MJB, et al. Radiotherapy plus concomitant and adjuvant temozolomide for glioblastoma. N Engl J Med. 2005;352(10):987–96.
3. Muldoon LL, Soussain C, Jahnke K, Johanson C, Siegal T, Smith QR, et al. Chemotherapy delivery issues in central nervous system malignancy: a reality check. J Clin Oncol Off J Am Soc Clin Oncol. 2007;25(16):2295–305.
4. Zalutsky MR, Reardon DA, Akabani G, Coleman RE, Friedman AH, Friedman HS, et al. Clinical experience with alpha-particle emitting 211At: treatment of recurrent brain tumor patients with 211At-labeled chimeric antitenascin monoclonal antibody 81C6. J Nucl Med Off Publ Soc Nucl Med. 2008;49(1):30–8.
5. Reardon DA, Akabani G, Coleman RE, Friedman AH, Friedman HS, Herndon JE, et al. Phase II trial of murine (131)I-labeled antitenascin monoclonal antibody 81C6 administered into surgically created resection cavities of patients with newly diagnosed malignant gliomas. J Clin Oncol Off J Am Soc Clin Oncol. 2002;20(5):1389–97.
6. Reardon DA, Rich JN, Friedman HS, Bigner DD. Recent advances in the treatment of malignant astrocytoma. J Clin Oncol Off J Am Soc Clin Oncol. 2006;24(8):1253–65.
7. Veeravagu A, Liu Z, Niu G, Chen K, Jia B, Cai W, et al. Integrin alphavbeta3-targeted radioimmunotherapy of glioblastoma multiforme. Clin Cancer Res Off J Am Assoc Cancer Res. 2008;14(22):7330–9.
8. Casacó A, López G, García I, Rodríguez JA, Fernández R, Figueredo J, et al. Phase I single-dose study of intracavitary-administered Nimotuzumab labeled with 188 Re in adult recurrent high-grade glioma. Cancer Biol Ther. 2008;7(3):333–9.
9. Sofou S, Thomas JL, Lin H, McDevitt MR, Scheinberg DA, Sgouros G. Engineered liposomes for potential alpha-particle therapy of metastatic cancer. J Nucl Med Off Publ Soc Nucl Med. 2004;45(2):253–60.
10. Phillips WT, Goins B, Bao A, Vargas D, Guttierez JE, Trevino A, et al. Rhenium-186 liposomes as convection-enhanced nanoparticle brachytherapy for treatment of glioblastoma. Neuro-Oncol. 2012;14(4):416–25.
11. Huang F-YJ, Lee T-W, Kao C-HK, Chang C-H, Zhang X, Lee W-Y, et al. Imaging, autoradiography, and biodistribution of (188)Re-labeled PEGylated nanoliposome in orthotopic glioma bearing rat model. Cancer Biother Radiopharm. 2011;26(6):717–25.
12. Heurtault B, Saulnier P, Pech B, Proust J-E, Benoit J-P. A novel phase inversion-based process for the preparation of lipid nanocarriers. Pharm Res. 2002;19(6):875–80.
13. Allard E, Hindre F, Passirani C, Lemaire L, Lepareur N, Noiret N, et al. 188Re-loaded lipid nanocapsules as a promising radiopharmaceutical carrier for internal radiotherapy of malignant gliomas. Eur J Nucl Med Mol Imaging. 2008;35(10):1838–46.
14. Vanpouille-Box C, Lacoeuille F, Belloche C, Lepareur N, Lemaire L, LeJeune J-J, et al. Tumor eradication in rat glioma and bypass of immunosuppressive barriers using internal radiation with (188)Re-lipid nanocapsules. Biomaterials. 2011;32(28):6781–90.
15. Vescovi AL, Galli R, Reynolds BA. Brain tumour stem cells. Nat Rev Cancer. 2006;6(6):425–36.
16. Singh SK, Clarke ID, Terasaki M, Bonn VE, Hawkins C, Squire J, et al. Identification of a cancer stem cell in human brain tumors. Cancer Res. 2003;63(18):5821–8.
17. Singh SK, Hawkins C, Clarke ID, Squire JA, Bayani J, Hide T, et al. Identification of human brain tumour initiating cells. Nature. 2004;432(7015):396–401.
18. Galli R, Binda E, Orfanelli U, Cipelletti B, Gritti A, De Vitis S, et al. Isolation and characterization of tumorigenic, stem-like neural precursors from human glioblastoma. Cancer Res. 2004;64(19):7011–21.
19. Sanai N, Alvarez-Buylla A, Berger MS. Neural stem cells and the origin of gliomas. N Engl J Med. 2005;353(8):811–22.
20. Schonberg DL, Lubelski D, Miller TE, Rich JN. Brain tumor stem cells: Molecular characteristics and their impact on therapy. Mol Aspects Med. 2014;39:82–101.
21. Bao S, Wu Q, Li Z, Sathornsumetee S, Wang H, McLendon RE, et al. Targeting cancer stem cells through L1CAM suppresses glioma growth. Cancer Res. 2008;68(15):6043–8.
22. Bao S, Wu Q, Sathornsumetee S, Hao Y, Li Z, Hjelmeland AB, et al. Stem cell-like glioma cells promote tumor angiogenesis through vascular endothelial growth factor. Cancer Res. 2006;66(16):7843–8.
23. Cheng L, Wu Q, Huang Z, Guryanova OA, Huang Q, Shou W, et al. L1CAM regulates DNA damage checkpoint response of glioblastoma stem cells through NBS1. EMBO J. 2011;30(5):800–13.
24. Singh AK, Arya RK, Trivedi AK, Sanyal S, Baral R, Dormond O, et al. Chemokine receptor trio: CXCR3, CXCR4 and CXCR7 crosstalk via CXCL11 and CXCL12. Cytokine Growth Factor Rev. 2013;24(1):41–9.
25. Zhang J, Sarkar S, Yong VW. The chemokine stromal cell derived factor-1 (CXCL12) promotes glioma invasiveness through MT2-matrix metalloproteinase. Carcinogenesis. 2005;26(12):2069–77.
26. Ehtesham M, Mapara KY, Stevenson CB, Thompson RC. CXCR4 mediates the proliferation of glioblastoma progenitor cells. Cancer Lett. 2009;274(2):305–12.
27. Brown JM. Vasculogenesis: a crucial player in the resistance of solid tumours to radiotherapy. Br J Radiol. 2014;87(1035):20130686.
28. Ahn G-O, Brown JM. Matrix metalloproteinase-9 is required for tumor vasculogenesis but not for angiogenesis: role of bone marrow-derived myelomonocytic cells. Cancer Cell. 2008;13(3):193–205.
29. Tseng D, Vasquez-Medrano DA, Brown JM. Targeting SDF-1/CXCR4 to inhibit tumour vasculature for treatment of glioblastomas. Br J Cancer. 2011;104(12):1805–9.
30. Kioi M, Vogel H, Schultz G, Hoffman RM, Harsh GR, Brown JM. Inhibition of vasculogenesis, but not angiogenesis, prevents the recurrence of glioblastoma after irradiation in mice. J Clin Invest. 2010;120(3):694–705.
31. Barbero S, Bonavia R, Bajetto A, Porcile C, Pirani P, Ravetti JL, et al. Stromal cell-derived factor 1alpha stimulates human glioblastoma cell growth through the activation of both extracellular signal-regulated kinases 1/2 and Akt. Cancer Res. 2003;63(8):1969–74.
32. Lepareur N, Garin E, Noiret N, Herry JY. A kit formulation for the labelling of lipiodol with generator-produced Re-188. J Label Compd Radiopharm. 2004;47(12):857–67.
33. Bourseau-Guilmain E, Béjaud J, Griveau A, Lautram N, Hindré F, Weyland M, et al. Development and characterization of immuno-nanocarriers targeting the cancer stem cell marker AC133. Int J Pharm. 2012;423(1):93–101.
34. Sharonov S, Chourpa I, Morjani H, Nabiev I, Manfait M, Feofanov A. Confocal Spectral Imaging Analysis in Studies of the Spatial-Distribution of Antitumor Drugs Within Living Cancer-Cells. Anal Chim Acta. 1994;290(1–2):40–7.
35. Vibet S, Mahéo K, Goré J, Dubois P, Bougnoux P, Chourpa I. Differential subcellular distribution of mitoxantrone in relation to chemosensitization in two human breast cancer cell lines. Drug Metab Dispos Biol Fate Chem. 2007;35(5):822–8.
36. Hirsjärvi S, Sancey L, Dufort S, Belloche C, Vanpouille-Box C, Garcion E, et al. Effect of particle size on the biodistribution of lipid nanocapsules: comparison between nuclear and fluorescence imaging and counting. Int J Pharm. 2013;453(2):594–600.
37. Fluckiger Laurence. Intérêt des nanosphères comme forme orale à libération modifiée pour améliorer la biodisponibilité et le profil pharmacodynamique de l'isradipine. Université Henri Poincaré - Nancy 1; 1999.
38. Allard E, Passirani C, Benoit J-P. Convection-enhanced delivery of nanocarriers for the treatment of brain tumors. Biomaterials. 2009;30(12):2302–18.
39. Biswas SK, Mantovani A. Macrophage plasticity and interaction with lymphocyte subsets: cancer as a paradigm. Nat Immunol. 2010;11(10):889–96.
40. Torres LA, Coca MA, Batista JF, Casaco A, Lopez G, García I, et al. Biodistribution and internal dosimetry of the 188Re-labelled humanized monoclonal antibody anti-epidemal growth factor receptor, nimotuzumab, in

the locoregional treatment of malignant gliomas. Nucl Med Commun. 2008;29(1):66–75.
41. Tarasova NI, Stauber RH, Michejda CJ. Spontaneous and ligand-induced trafficking of CXC-chemokine receptor 4. J Biol Chem. 1998;273(26):15883–6.
42. Tanabe S, Heesen M, Yoshizawa I, Berman MA, Luo Y, Bleul CC, et al. Functional expression of the CXC-chemokine receptor-4/fusin on mouse microglial cells and astrocytes. J Immunol Baltim Md 1950. 1997;159(2):905–11.
43. Zagzag D, Lukyanov Y, Lan L, Ali MA, Esencay M, Mendez O, et al. Hypoxia-inducible factor 1 and VEGF upregulate CXCR4 in glioblastoma: implications for angiogenesis and glioma cell invasion. Lab Investig J Tech Methods Pathol. 2006;86(12):1221–32.
44. Ma Y-H, Mentlein R, Knerlich F, Kruse M-L, Mehdorn HM, Held-Feindt J. Expression of stem cell markers in human astrocytomas of different WHO grades. J Neurooncol. 2008;86(1):31–45.
45. Ehtesham M, Winston JA, Kabos P, Thompson RC. CXCR4 expression mediates glioma cell invasiveness. Oncogene. 2006;25(19):2801–6.
46. Hardee ME, Zagzag D. Mechanisms of glioma-associated neovascularization. Am J Pathol. 2012;181(4):1126–41.
47. Mignogna C, Signorelli F, Vismara MFM, Zeppa P, Camastra C, Barni T, et al. A reappraisal of macrophage polarization in glioblastoma: Histopathological and immunohistochemical findings and review of the literature. Pathol Res Pract. 2016;212(6):491–9.
48. Pyonteck SM, Akkari L, Schuhmacher AJ, Bowman RL, Sevenich L, Quail DF, et al. CSF-1R inhibition alters macrophage polarization and blocks glioma progression. Nat Med. 2013;19(10):1264–72.
49. Saha D, Martuza RL, Rabkin SD. Macrophage Polarization Contributes to Glioblastoma Eradication by Combination Immunovirotherapy and Immune Checkpoint Blockade. Cancer Cell. 2017;32(2):253–267.e5.
50. Béduneau A, Saulnier P, Hindré F, Clavreul A, Leroux J-C, Benoit J-P. Design of targeted lipid nanocapsules by conjugation of whole antibodies and antibody Fab' fragments. Biomaterials. 2007;28(33):4978–90.
51. Bobo RH, Laske DW, Akbasak A, Morrison PF, Dedrick RL, Oldfield EH. Convection-enhanced delivery of macromolecules in the brain. Proc Natl Acad Sci U S A. 1994;91(6):2076–80.
52. Ling CC, Humm J, Larson S, Amols H, Fuks Z, Leibel S, et al. Towards multidimensional radiotherapy (MD-CRT): biological imaging and biological conformality. Int J Radiat Oncol Biol Phys. 2000;47(3):551–60.
53. Hall EJ. Dose-painting by numbers: a feasible approach? Lancet Oncol. 2005;6(2):66.
54. Supiot S, Lisbona A, Paris F, Azria D, Fenoglietto P. « Dose-painting » : mythe ou réalité ? Cancer/Radiothérapie. 2010;14(6–7):554–62.
55. Chan AA, Lau A, Pirzkall A, Chang SM, Verhey LJ, Larson D, et al. Proton magnetic resonance spectroscopy imaging in the evaluation of patients undergoing gamma knife surgery for Grade IV glioma. J Neurosurg. 2004;101(3):467–75.
56. Grosu AL, Weber WA, Franz M, Stärk S, Piert M, Thamm R, et al. Reirradiation of recurrent high-grade gliomas using amino acid PET (SPECT)/CT/MRI image fusion to determine gross tumor volume for stereotactic fractionated radiotherapy. Int J Radiat Oncol Biol Phys. 2005;63(2):511–9.
57. Lemée J-M, Clavreul A, Menei P. Intratumoral heterogeneity in glioblastoma: don't forget the peritumoral brain zone. Neuro-Oncol. 2015;17(10):1322–32.
58. Petrecca K, Guiot M-C, Panet-Raymond V, Souhami L. Failure pattern following complete resection plus radiotherapy and temozolomide is at the resection margin in patients with glioblastoma. J Neurooncol. 2013;111(1):19–23.
59. Bouras A, Kaluzova M, Hadjipanayis CG. Radiosensitivity enhancement of radioresistant glioblastoma by epidermal growth factor receptor antibody-conjugated iron-oxide nanoparticles. J Neurooncol. 2015;124(1):13–22.
60. Kaluzova M, Bouras A, Machaidze R, Hadjipanayis CG. Targeted therapy of glioblastoma stem-like cells and tumor non-stem cells using cetuximab-conjugated iron-oxide nanoparticles. Oncotarget. 2015;6(11):8788–806.
61. Merlo A, Jermann E, Hausmann O, Chiquet-Ehrismann R, Probst A, Landolt H, et al. Biodistribution of 111In-labelled SCN-bz-DTPA-BC-2 MAb following loco-regional injection into glioblastomas. Int J Cancer. 1997;71(5):810–6.
62. Séhédic D, Cikankowitz A, Hindré F, Davodeau F, Garcion E. Nanomedicine to overcome radioresistance in glioblastoma stem-like cells and surviving clones. Trends Pharmacol Sci. 2015;36(4):236–52.
63. Chau N-M, Rogers P, Aherne W, Carroll V, Collins I, McDonald E, et al. Identification of novel small molecule inhibitors of hypoxia-inducible factor-1 that differentially block hypoxia-inducible factor-1 activity and hypoxia-inducible factor-1alpha induction in response to hypoxic stress and growth factors. Cancer Res. 2005;65(11):4918–28.
64. Miao Z, Luker KE, Summers BC, Berahovich R, Bhojani MS, Rehemtulla A, et al. CXCR7 (RDC1) promotes breast and lung tumor growth in vivo and is expressed on tumor-associated vasculature. Proc Natl Acad Sci U S A. 2007;104(40):15735–40.
65. Wuerth R, Bajetto A, Harrison JK, Barbieri F, Florio T. CXCL12 modulation of CXCR4 and CXCR7 activity in human glioblastoma stem-like cells and regulation of the tumor microenvironment. Front Cell Neurosci. 2014;8:144.
66. Walters MJ, Ebsworth K, Berahovich RD, Penfold MET, Liu S-C, Al Omran R, et al. Inhibition of CXCR7 extends survival following irradiation of brain tumours in mice and rats. Br J Cancer. 2014;110(5):1179–88.
67. Brown JM. Inhibiting Vasculogenesis After Radiation: A New Paradigm to Improve Local Control by Radiotherapy. Semin Radiat Oncol. 2013;23(4):281–7.
68. Herrmann K, Schottelius M, Lapa C, Osl T, Poschenrieder A, Hänscheid H, et al. First-in-Human Experience of CXCR4-Directed Endoradiotherapy with 177Lu- and 90Y-Labeled Pentixather in Advanced-Stage Multiple Myeloma with Extensive Intra- and Extramedullary Disease. J Nucl Med Off Publ Soc Nucl Med. 2016;57(2):248–51.

Supplemental Figure S1: Analysis of immunoreactivity of free 12G5 antibody and 12G5-LNCs as a function of time after storage at 4°C determined by flow cytometry on U87MG transfected cells. The free 12G5 antibody and 12G5-LNCs labeled U87MG CXCR4+ cells. 12G5-LNCs labeling remains stable for 3 days. Statistical analysis was performed with the log-rank test (* $p < 0.05$; ** $p < 0.001$).

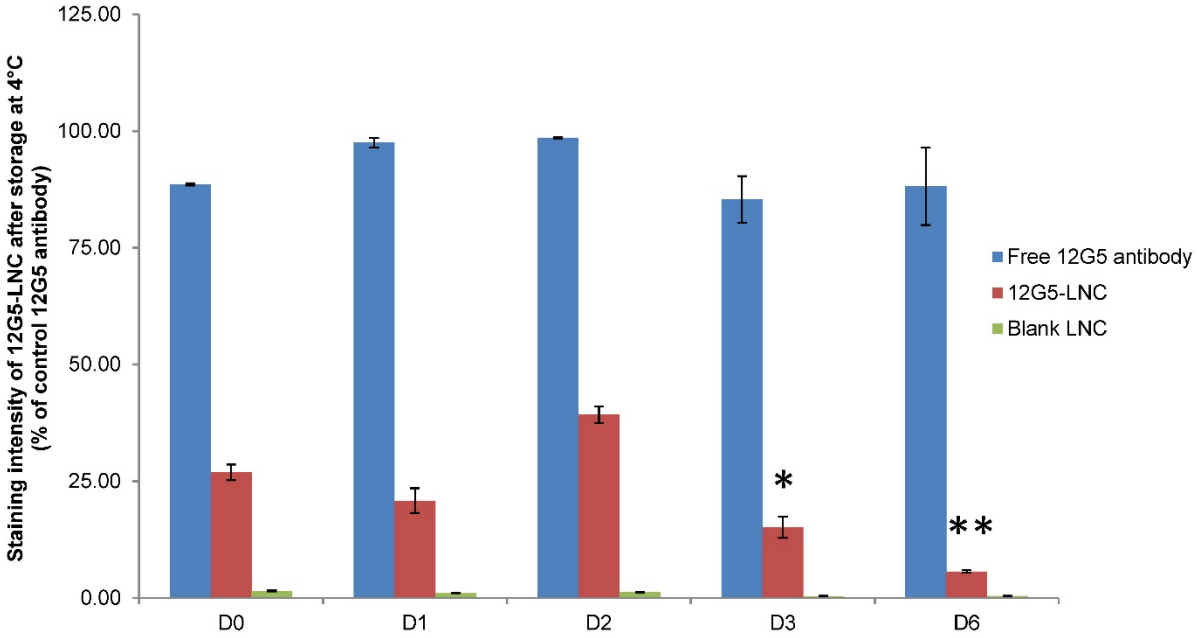

Supplemental Figure S2: Western blot analysis of the phosphorylation of Akt in U87MG CXCR4+ cells 16 hours after stimulation by SDF-1 at 25nM depending from the presence of LNC formulations (12G5-LNC, IgG2a-LNCs and LNCs) or not (PBS).